Cement and Concrete Research 151 (2022) 106585

Contents lists available at ScienceDirect

Cement and Concrete Research

journal homepage: www.elsevier.com/locate/cemconres

A structurally-consistent CASH+ sublattice solid solution model for fully hydrated C-S-H phases: Thermodynamic basis, methods, and Ca-Si-H_2O core sub-model

Dmitrii A. Kulik [a,*], George Dan Miron [a], Barbara Lothenbach [b]

[a] Laboratory for Waste Management, Paul Scherrer Institut, Forschungsstrasse 111, 5232 Villigen PSI, Switzerland
[b] Laboratory Concrete & Asphalt, Empa, Dubendorf, Switzerland

ARTICLE INFO

Keywords:
Calcium silicate hydrates
C-S-H
Cation uptake
Thermodynamic modelling
Sublattice solid solutions

ABSTRACT

A new thermodynamic model, CASH+, is proposed, aimed at accurately describing equilibrium composition, stability, solubility, and density of C-S-H gel-like phases at varying chemical conditions. Taking advantage from recent atomistic and spectroscopic studies, this sublattice solid solution model allows incremental extensions to accommodate alkali, aluminum and other cations. This incrementality, achieved first time for a C-S-H solid solution model, means that all thermodynamic properties of endmembers and interaction parameters can be kept fixed in further extensions. This paper describes principles of how endmembers of CASH+ solid solution model can be constructed by permutating moieties assigned to different sublattices, and how the structural consistency of the model can be established. Initial standard thermodynamic properties of endmembers were estimated using predictive methods and PSI/Nagra and Cemdata18 chemical thermodynamic databases. The parameterized core CASH+ sub-model in Ca-Si-H_2O system is shown to perform well in presence of liquid water at temperatures up to 90 °C.

1. Introduction

Calcium silicate hydrate (C-S-H) phases of variable composition determine the most relevant properties and the durability of hydrated cement pastes and concretes ([1,2] and references therein). There is an urgent need for accurate chemical thermodynamic prediction of stability, density, solubility and composition of C-S-H (including water content and uptake of minor cations Na, K, Li, Al, Fe, Sr, Ba, U, …), in response to changes in cement recipe, water/binder ratio, temperature, carbonation, leaching, and other factors. Resolving this problem is a major challenge in cement chemistry in general, and in the use of cement materials as a waste matrix or repository backfill in particular. Hence, it is not surprising that many alternative thermodynamic models of C-S-H have been proposed and applied to C-S-H solubility data with various degrees of success (see an overview in Walker et al. [2]). Among those, the solid solution models of different complexity belong to the most popular group, to which the authors have contributed too [3–5]. In recent years, the desire to make C-S-H solid solution models more consistent with the atomistic structure also became more evident [4,6,7].

There is a vast and growing evidence that C-S-H particles have a so-called defect tobermorite structure [8–11] derived from that of 14 Å or 11 Å tobermorite. The structure of tobermorite $Ca_5Si_6O_{16}(OH)_2{\cdot}7H_2O$ is composed of calcium oxide sheets packed between "dreierketten" silicate chains [12]. The deprotonation of silanol groups on silicate chains creates negative charges that are compensated by Ca^{2+} or other cations entering the interlayer spaces together with water molecules. The cross-linking between the bridging tetrahedra may occur at low C/S (Ca/Si molar ratios) [11] or at elevated temperatures [13], which may reduce the interlayer charge.

Recent atomistic simulations ([14,15] and references therein) suggest that most, if not all, varieties and compositions of C-S-H can be derived from 14 Å- or 11 Å-tobermorite structures by introducing various defects, i.e. substitutions of silica by other moieties or vacancies at bridging tetrahedral BT sites, as well as by the related (via the charge balance) cation- or vacancy substitutions at interlayer cationic IC sites. The non-gel water content of C-S-H also depends upon a substitution of H_2O by vacancy at interlayer water IW sites in response to relative humidity (Fig. 1).

In chemical thermodynamic terms, the formation of defects such as

* Corresponding author.
E-mail address: dmitrii.kulik@psi.ch (D.A. Kulik).

https://doi.org/10.1016/j.cemconres.2021.106585
Received 20 November 2020; Received in revised form 23 August 2021; Accepted 25 August 2021
Available online 7 October 2021

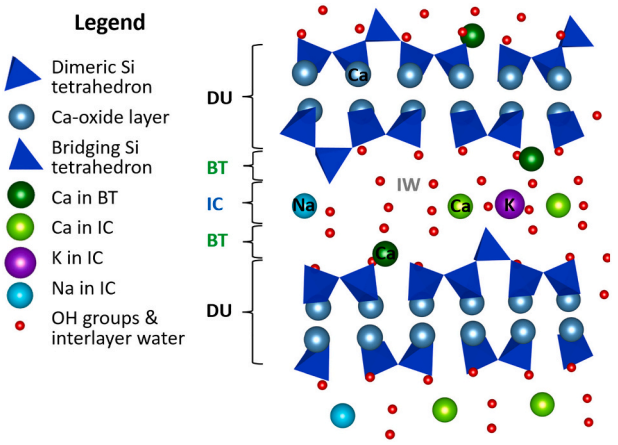

Fig. 1. Schematic C-S-H structure based on the tobermorite model with defects in silicate chains. Oxygens are not shown for simplicity. The model includes sublattices: IW: Interlayer Water (species: H_2O, Va); BT: Bridging Tetrahedral (Si, Al, Ca, Va); IC: Interlayer Cation (Ca, K, Na, Va). DU: dimeric units each made of a silica dimer bound via common oxygen to two calcium atoms from the Ca-oxide layer. Va stands for a vacancy.

substitutions of structural moieties by cations, anions or vacancies, can be conveniently expressed by considering C-S-H as a sublattice solid solution, where the mixing occurs simultaneously in two or three sublattices [4]. A sublattice stands for a set of all structural sites of the same type in the (crystal) structure [16,17]. Sublattice models reflect a certain kind of long-range ordering; this renders them some extent of consistency with the atomistic structure of the solid. For this reason, such models are expected to be more flexible, predictive, and incremental than semi-empirical solid solution models downscaled to the simple single-site mixing e.g. in [3,4,6]. A detailed description of terms and concepts behind sublattice solid solution models, representation of substituting moieties and endmembers, and equations for calculation of properties of mixing are provided in Appendix A1 (Supporting Material) for convenience of a thoughtful reader.

The drawbacks of previously developed solid solution models of C-S-H include the lack of incrementality in extending the model by adding a new cation such as Na^+ or Al^{3+}. In this case, not just the part for newly-added endmembers and interaction parameters, but the whole model (i.e. standard chemical potentials of endmembers, possibly together with interaction parameters of mixing) may need to be re-parameterized. Recognition of this shortage was our main motivation for developing a new, incrementally extendable and more structurally consistent CASH+ sublattice solid solution model. As claimed in [7,18], this model (still called CNKASH then) is capable of describing composition, solubility, density, non-gel water content, and mean silicate chain length (MCL) in a wide range of compositions.

This paper aims at communicating main features of the CASH+ sublattice solid solution model to lay down the foundation for its initial parameterization and subsequent incremental extensions in companion publications. Other objectives include:

- Selection of sublattice moieties based on structural and atomistic features of C-S-H;
- Construction of endmembers and initial estimation of their standard thermodynamic properties;
- Setup of Berman-type sublattice solid solution model with site-specific non-ideality, its thermodynamic basis, and implementation in GEM-Selektor and PHREEQC codes;
- Parameterization of CASH+ core sub-model in Ca-Si-H_2O subsystem and demonstration of its behaviour in comparison with the selected experimental data on C-S-H solubility;
- Discussion of density and temperature trends, as well as approaches for the extension, verification, and potential applications of the CASH+ model.

2. The CASH+ model and its underlying assumptions

The atomistic structure of C-S-H phases is complex and involves various defects of the tobermorite structure that occur depending on the composition expressed by C/S ratio [15,19], which also affects the interlayer distance (11 Å to 14 Å). In principle, any atomic unit or cell identified by Kunhi Mohamed et al. [15] can be considered as a moiety for the sublattice solid solution model. However, this would result in a huge number of possible endmembers, which would make the thermodynamic model intractable in a practical sense. Hence, we have elaborated some assumptions and rules to minimize the number of sublattices and endmembers, thus making the solid solution model as simple as possible, while retaining its maximum flexibility and its consistency to major structural features. These assumptions define (a) distribution of electric charge between BT (bridging tetrahedral) and IC (interlayer cationic) sublattices and their moieties; and (b) the stoichiometry of moieties that can substitute each other on BT, IC and IW (interlayer water) sublattices.

2.1. Assumptions behind the CASH+ model

Assumption (1), supported by the results of atomistic simulations by Churakov et al. [20,21], consists in that the charges acting on IC sites originate at BT sites due to a partial deprotonation of silanol OH^- groups existing on bonds stemming either from bridging silicon (or aluminum) or from dimeric silicon atoms. In the CASH+ model development, this assumption translates into a rule that any moiety in permanent-charge BT (bridging tetrahedral) sites has charge of −1, and any moiety compensating the charge in the BT moiety or in the vicinity of it has charge of +1. This means that for each BT site, there is an IC (interlayer cationic) site containing a counter-ion of charge +1. Any moiety in IW (interlayer water) sites is assumed to be electrically neutral. Although being a strong simplification of the rather complex reality, this rule guarantees that any endmember constructed by a permutation of moieties on any of the three sublattices will be automatically electroneutral, which greatly simplifies the construction of endmembers and the treatment of non-ideality in the mixing model.

A more complex reality is depicted in a variety of structural defects identified by Kunhi Mohamed et al. [15]. Their "building blocks" always include two dimers located on both sides of the interlayer. Regarding the defects in such a building block, it is possible to have one Ca^{2+} ion that compensates negative charges of BT moieties on both sides of the interlayer. Accounting for such cases by introducing different Ca moieties in IC sites, or different IC sublattices, with some moieties containing fractional number of Ca atoms, would make our solid solution model far too complex. To keep the model simple, we decided to neglect such details and depict the Ca^{2+} moiety in the IC site as $CaH(OH)_2^+$, formally a $Ca(OH)^+$ complex with one H_2O molecule, added for making the model compliant with the known non-gel H_2O content as function of C/S ratio. This simplification of atomistic reality can be partially compensated by strong non-ideal interactions on the IC site, evident after the model parameterization. Similar to models for cation exchange in clays, our moieties substituting each other in IC sublattice, include one cation per site independently of the charge of the cation. The moieties for Na^+ or K^+ retain charge of +1, and include one H_2O molecule (for correct H_2O content).

As shown in [15], and as needed to reach C/S > 1.5, calcium *must* enter the BT sublattice, probably as Ca^{2+} ion surrounded by two OH^- groups. This would lead to a moiety formula $Ca(OH)_2^0$, but according to our rule of charges, we have to simplify this to $CaOOH^-$. Note that this calcium moiety, assigned to BT sites, embraces also three other configurations identified in [15]: two involving another Ca^{2+} cation, and one

missing the OH^- groups. In the thermodynamic model, this simplification is expected to be compensated by strong non-ideal interactions between different moieties in BT sublattice.

Assumption (2) is that exchange cations in the IC (interlayer cationic) sites retain part of their hydration shell when entering the interlayer from the pore solution. This idea allows defining the formulae of some IC moieties in a way that the model can correctly reproduce the solid (non-gel) water content in C-S-H at least in the presence of liquid water. In most cases, it turns out that one H_2O molecule needs to be included into the formula of a cationic moiety.

Assumption (3), reflecting the tobermorite structure of C-S-H, is that any endmember formula must include a fragment of that structure involving a silicate dimer $Si_2O_7^{6-}$ with two charge-compensating Ca^{2+} and two H^+ ions, comprising a formally neutral 'T' moiety $[Ca_2Si_2O_5(OH)_2]^0$. This is convenient because of the known fact (obtained from ^{27}Si NMR spectroscopy [22]) that the monomeric silica is practically absent from C-S-H, even for the most depolymerized samples with the highest C/S ratio, where the dimeric silica prevails [1,15,23]. We further assume that only 'T' moiety can occupy the DU (dimeric unit) site, which excludes the DU sublattice from considering in the mixing, thus much simplifying the whole thermodynamic model of sublattice solid solution (see below).

Per one dimeric 'T' unit forming the DU structural site, one BT (bridging-tetrahedral) site must exist (see Fig. 1). When this BT site is vacant (e.g. not occupied by silica, aluminum etc.), it embraces two silanol groups on dimeric silica tetrahedra, at least one of which is deprotonated. This type of vacancy can be formally represented as an OH^- moiety (denoted as 'v' = vacant) in the BT site. When the BT site is occupied by silica forming a piece of "dreierkette", this moiety can be represented by a SiO_2OH^- formula. In a structural sense, this kind of BT moiety can be imagined as a silicate tetrahedron connected to two adjacent dimers and exposing two silanol groups into the interlayer, one of which is deprotonated and carries a negative charge.

If a BT site is occupied by aluminum in tetrahedral coordination, it is expected to be an aluminate tetrahedron with two bonds sharing oxygen with the adjacent silicate dimers, and two Al-OH groups, together carrying charge of −1. Therefore, the Al(IV) moiety formula in BT site can be written as $AlO(OH)_2^-$. Note that Kunhi Mohamed et al. [14] did not corroborate the existence of an interlayer cationic species of aluminum, assigning spectroscopic and atomistic observations of Al(IV), Al(V) and Al(VI) in C-S-H to BT sites. We follow their idea in part and assume the same BT species for all three cases of Al coordination for model simplicity and consistency.

Assumption (4) behind the CASH+ model is that there is one IW (interlayer water) site per one T dimer in DU site, and in the presence of liquid water, all the IW sites are occupied with 'h' moieties (H_2O molecules). At low relative humidity, part of IW sites may be vacant (i.e. occupied by a true vacancy Va 'v'). All further considerations assume that the liquid water is present, and, therefore, the IW sublattice does not contribute to the properties of mixing.

2.2. Definition of the CASH+ model

With the above assumptions and rules, possible endmembers of the CASH+ solid solution can be constructed by a permutation of moieties using a template formula [DU]:BT:IC:IW:, where [DU] is a constant dimeric unit of the tobermorite structure, always occupied by 'T' moiety, and IW site is occupied by H_2O or vacancy. Moieties and vacancies in BT and IC sites (Table 1) are chosen to produce only charge-compensated endmembers, and to yield realistic non-gel water contents at full hydration in presence of liquid water and C/S ratios varying between 0.67 and 2.0. The vacancy 'Va' in IW sites will not be used further in this study: it was added for future extensions of the model to cover partially dried C-S-H phases. More technicalities on constructing CASH+ endmembers are provided in Section 2.3.

The backbone of CASH+ sublattice solid solution model (Table 1) comprises quite a significant simplification of the complex atomistic reality of the defect tobermorite structure of C-S-H. This simplification should be understood as a balance act aimed at providing enough structural detail and flexibility, but keeping the sublattice solid solution model still tractable, relatively simple and compact.

In the following sections, we will focus on constructing and parameterizing the CASH+ core sub-model for the Ca-Si-H_2O system. Further extensions of this core model with endmembers and interaction parameters for alkali- and alkali-earth metals uptake will be presented and parameterized in Miron et al. [24]; on top of that, the extensions for Al^{III} and Fe^{III} uptake will be provided in Miron et al. [25]; and extensions for the uptake of cations of environmental concern (heavy metals, REE, actinides) will be described in Miron et al. [26]. Accordingly, the tables with endmembers, their thermodynamic properties, and interaction parameters will be incrementally extended in those papers, and in parallel will be made provisionally available from the authors as future extensions to Cemdata18 [27] and PSI-Nagra [28] chemical thermodynamic databases for GEMS codes. The moieties including those for Na, K, Al and Fe are listed in Table 1 to provide the reader with an integral view of the whole model. The name "CASH+" reflects the fact that aluminum is an essential minor component of C-S-H phases in almost any practically used hydrated cement, and that reaching an accurate model of Al incorporation in C-S-H was the ultimate goal of two research projects resulting in this contribution and its companion papers.

2.3. Generating CASH+ core sub-model endmembers

All possible endmembers of the CASH+ model can be generated by permutation, which combines one moiety per each sublattice. In Table 2, this principle is illustrated by six endmembers of the CASH+ core sub-model; other generated endmembers for Na, K, Al, Fe will be added and considered in companion papers. For the easier identification in the endmember names, each moiety is coded with one letter 'T', 'S', 'v', 'C', 'h' (see Table 1). For instance, the endmember with minimal C/S = 0.67 (see the second row in Table 2) has the name "TSvh", and its chemical formula is composed of four respective moieties: $[Ca_2Si_2O_5(OH)_2]$,

Table 1
Sublattice sites and main moieties defining the CASH+ solid solution model.

Sites	DU (dimeric unit)		BT (bridging tetrahedral)		IC (interlayer cation)		IW (interlayer water)	
Site multiplicity		1		1		1		1
Moieties (species)	$[Ca_2Si_2O_5(OH)_2]^0$	T	SiO_2OH^-	S	H^+	v	H_2O	h
			OH^-	v	$CaH(OH)_2^+$	C	Va	v
			$CaOOH^-$	C	$NaHOH^+$	N		
			$Al(OH)_4^-$	A	$KHOH^+$	K		
			$Fe(OH)_4^-$	F	$FeH(OH)_3^+$	F		
			Other	…	Other	…		

For a fully hydrated state (in presence of liquid water), the vacancy Va 'v' in IW site is not considered (i.e. no substitution in IW sites so far, Va shown for completeness) Fe^{III} is assumed to enter both BT and IC sublattices. Letters 'T', 'S', 'v', 'C', 'N', 'K', 'A', 'F', 'h' and so on are codes of respective moieties used in short names of generated endmembers (Table 2). Vacancy 'v' is represented by OH- in BT sites and by H+ in IC sites.

Table 2
Endmembers of the CASH+ core model, generated by permutating moieties on BT and IC sites.[a]

End-members	Sites and sublattice formula moieties				CL	C/S	H/S
	DU	BT	IC	IW			
T S v h	$[Ca_2Si_2O_5(OH)_2]$	SiO_2OH^-	H^+	H_2O	∞	2/3	1
T S C h	$[Ca_2Si_2O_5(OH)_2]$	SiO_2OH^-	$CaH(OH)_2^+$	H_2O	∞	1	4/3
T v v h	$[Ca_2Si_2O_5(OH)_2]$	OH^-	H^+	H_2O	2	1	3/2
T C v h	$[Ca_2Si_2O_5(OH)_2]$	$CaOOH^-$	H^+	H_2O	2	3/2	3/2
T v C h	$[Ca_2Si_2O_5(OH)_2]$	OH^-	$CaH(OH)_2^+$	H_2O	2	3/2	2
T C C h	$[Ca_2Si_2O_5(OH)_2]$	$CaOOH^-$	$CaH(OH)_2^+$	H_2O	2	2	2

[a] Sublattice sites with substituting moieties are indicated by colons ':'. DU: Dimeric unit of tobermorite (T) structure, always occupied by 'T' moiety $[Ca_2Si_2O_5(OH)_2]^0$; BT: bridging tetrahedral site; IC: the interlayer cation site; IW: the interlayer water site, always occupied by the 'h' moiety $\{H_2O\}$; CL: theoretical (alumino)silicate chain length in pure endmember; mole ratios: C/S: Ca/Si; H/S: H_2O/Si.

SiO_2OH^-, H^+, H_2O (Eq. (1)).

$$\underset{T}{\underset{\text{DU}}{[Ca_2Si_2O_5(OH)_2]}} : \underset{S}{\underset{\text{BT}}{\{SiO_2OH\}}} : \underset{v}{\underset{\text{IC}}{\{H\}}} : \underset{h}{\underset{\text{IW}}{\{H_2O\}}} \quad \textbf{TSvh} \tag{1}$$

Names and formulae of all endmembers are constructed from rows in Table 1 using the same template, maintaining the same order of sublattices: BT, IC and IW.

The TSvh endmember formally has the infinite silicate chain length $CL = \infty$, as any other compound with S or A moiety in the BT sublattice (Table 2). Any endmember with a vacancy, Ca, or other moiety except S or A in BT sublattice has $CL = 2$ and is called *dimeric*. The mean chain length MCL or $\langle CL \rangle$ can be easily estimated from the computed equilibrium speciation of C-S-H phase from the mole fractions x_j of dimeric endmembers ([4], Eq. (2)):

$$\langle CL \rangle = 3 \Big/ \sum_j x_j - 1,\ j \in (\text{dimeric endmembers}) \tag{2}$$

As the CASH+ model contains endmembers with $CL = \infty$ and with $CL = 2$, it can potentially reproduce any MCL $2 < \langle CL \rangle < \infty$ that can be measured in C-S-H by the NMR or FTIR spectroscopies.

2.4. Estimation of initial thermodynamic properties of endmembers

A typical feature of sublattice solid solution models is that they may consist of many endmembers, most of which do not exist as pure mineral substances. Hence, their standard thermodynamic properties cannot be derived from direct calorimetry or solubility data or collected from thermodynamic databases. However, to start parameter optimizations using GEMSFITS [29] or similar codes, at least the initial standard chemical potential μ^*_T (standard Gibbs energy per mole $g^*_T = \mu^*_T$) values of endmembers must lie within ±30 to ±50 kJ·mol^{-1} interval relative to their (yet unknown) "true" or "optimal" values. At larger uncertainty intervals, even global optimization algorithms may fail (based on our experience with the GEMSFITS code).

Besides, the solid solution model must correctly reproduce the known values of density, non-gel water content, enthalpy and heat

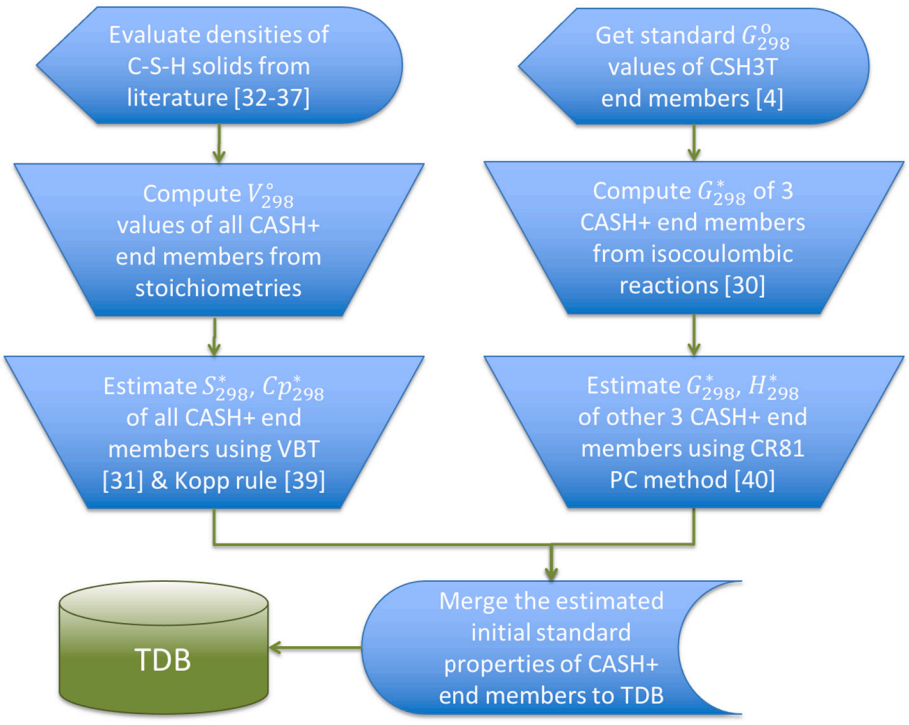

Fig. 2. Flow-chart for the initial estimation of standard thermodynamic properties of CASH+ core endmembers. VBT stands for "volume-based thermodynamics" [31]; CR81 PC – for "Chermak and Rimstidt 1981" [method of] polyhedral contributions [40]; TDB – for "thermodynamic database".

capacity of C-S-H phases, which means an urgent need for the consistent prediction/correlation of water stoichiometry, standard molar volume, absolute entropy, heat capacity and enthalpy for all possible endmembers. To meet all these needs in this work, we have developed a workflow (Fig. 2) that is described below.

The initial estimates of standard molar G^*_{298} values of CASH+ endmembers TSCh, TSvh, TCvh at $P_r = 1$ bar, $T_r = 298.15$ K (25 °C) were obtained from isocoulombic or isoelectric reactions [30] with $\Delta_r G^*_{298} = 0$, involving the T5C, T2C and TobH endmembers from our previous CSH3T model ([4], Tables 7, 8) while removing the "gel" water from the endmember stoichiometry. The initial G^*_{298} values of TvCh, TCCh, and Tvvh endmembers were subsequently estimated from the G^*_{298} values of TSvh and TCvh endmembers by adding H_2O or $Ca(OH)_2$,cr in the reaction with $\Delta_r G^*_{298} = 0$. The ReacDC module of GEM-Selektor code was used for calculations.

The standard values of entropy and heat capacity of C-S-H endmembers were estimated from their molar volumes using VBT (volume-based thermodynamics) equations [31], hence the densities of C-S-H have been considered. Since our last publication [4], more accurate data on densities of hydrated cement C-S-H and C-A-S-H (C/S about 1.7) were measured with ^{1}H NMR [32–34]. These studies limit the density of C-S-H without "gel pore water" to d = 2.6–2.8 g·cm^{-3}, in agreement with neutron scattering measurements in Allen et al. [35] that yielded d= 2.604 g·cm^{-3}. The neutron scattering study [36] reported a similar density of C-A-S-H (with C/S = 0.99, A/S = 0.06) from the alkali-activated slag paste, d = 2.73 g·cm^{-3}, which shows that densities of C-(A)-S-H may be quite similar at least in the range 0.99 < C/S < 1.7. Thomas et al. commented that "C-S-H formed from cement hydrated under normal conditions has a considerably higher atomic packing density than both tobermorite and jennite" [37]. They listed values d = 2.23 g·cm^{-3} for 1.4 nm tobermorite (C/S = 0.83, H/S = 1.33), and d = 2.48 g·cm^{-3} for 1.1 nm tobermorite (C/S = 0.75, H/S = 0.92), both significantly less than the values 2.6–2.8 g·cm^{-3} reported for C-S-H phases.

Direct measurements of C-S-H density at C/S < 0.9 are not yet available. The XRD data tend to indicate 1.2–1.4 nm tobermorite-like structure for low-Ca C-S-H and thus a density of ca. 2.4–2.5 g·cm^{-3}, with a decrease of basal spacing to 1.1–1.2 nm at increasing C/S ratio [9,11,38] which would correspond to higher densities >2.6–2.7 g·cm^{-3}. Hence, we can assume (based on the data summarized above) the density of 2.5 g·cm^{-3} for polymeric C-S-H with C/S < 0.75, while densities of C-S-H with C/S > 0.99 can be all set at 2.7 g·cm^{-3} with 0.1 g·cm^{-3} uncertainty.

The knowledge of density and molar volumes of C-S-H (endmembers) with a good accuracy is important for two reasons. Firstly, these values are needed to predict the chemical shrinkage upon cement hydration. Secondly, the accurate molar volumes can be used for predicting the standard values of entropy and heat capacity of C-S-H endmembers by applying the volume-based thermodynamics (VBT) [31].

Briefly, the VBT equations allow the determination of standard absolute entropy S°_{298} from the so-called formula unit volume $V_m = 10^{21} \cdot V^\circ_{298}/N_A$ in nm^3/(formula unit) (N_A = 6.022 • 10^{23} is Avogadro's number and V°_{298} is the molar volume in cm^3·mol^{-1}), and empirical constants k and c:

$$S^\circ_{298} = V_m k + c \ \left(\text{in J·mol}^{-1}\text{·K}^{-1}\right) \quad (3)$$

For hydrated ionic salts (to which C-S-H can belong) in Eq. (3), k = 1579 ± 30 and c = 6 ± 6, with the mean absolute error of S°_{298} estimate ±7.4 J·mol^{-1}·K^{-1} ([31], Table 2). A similar, though much less accurate VBT equation exists for the standard heat capacity:

$$Cp^\circ_{298} = V_m k' + c' \left(\text{in J·mol}^{-1}\text{·K}^{-1}\right) \quad (4)$$

Because C-S-H can be viewed as a non-framework silicate, in Eq. (4), k' = 1465 and c' = 11 ([31], Table 2). As these authors noted, the absolute error of such Cp°_{298} estimate is probably 25% of the value. Hence, we decided to compare the predictions from Eq. (4) with the Dulong-Petit limit for high-temperature heat capacity:

$$Cp^\circ_{298} = \text{m}\cdot 3R = \text{m}\cdot 25.0 \ \left(\text{in J·mol}^{-1}\text{·K}^{-1}\right) \quad (5)$$

where R = 8.31451 is the universal gas constant, and m is the number of atoms in the formula ([31], Table 1). In trial calculations, we found out that Dulong-Petit limit values from Eq. (5) are probably too high, up to 200 J·mol^{-1}·K^{-1} higher than those obtained from Eq. (4). Therefore, we tried next the modified Kopp rule of elemental contributions [39] based on the observation that Cp contributions of light elements are much less than 25 J·mol^{-1}·K^{-1}. This method estimates the heat capacity of a condensed substance as the sum of elements contributions:

$$Cp^\circ_{298} = \sum_i \text{m}_i Cp_i \ \left(\text{in J·mol}^{-1}\text{·K}^{-1}\right) \quad (6)$$

where m_i is the number of i-th element atoms in the substance formula, and Cp_i is the contribution per mole of i-th element (regressed from known heat capacities). Contributions for elements involved in C-S-H are: H: 7.56; O: 13.42; Si: 17.00; Ca: 28.25; K: 28.78; Na: 26.19; Al: 18.07; Fe: 29.08 (all in J·mol^{-1}·K^{-1}, from [39] Table 1). Values of Cp°_{298} calculated using Eq. (6) came out very similar to the respective values obtained from Eq. (4), indicating a good level of consistency. Hence, we decided to use Cp°_{298} estimates from Eq. (4) as acceptable initial estimates with 30% uncertainty. The necessary data are provided in Table 3. The obtained dataset of densities and VBT-estimated V°_{298}, S°_{298} and Cp°_{298} values for CASH+ core endmembers, with G^*_{298} estimates derived as described below, is provided in Table 4.

To further extend the initial standard thermodynamic dataset for CASH+ model with G^*_{298} estimates for endmembers containing other cations (also provided in companion papers) or not present in earlier models, we have used a simple method of polyhedral contributions by Chermak and Rimstidt [40] for estimating G^*_{298} and H^*_{298} values of minerals in the system Al-Si-Ca-Mg-Fe-Na-K-O-H. This method uses (regressed) contributions g_i to Gibbs energy and h_i to enthalpy of formation from elements (at 25 °C, 1 bar) from polyhedral units like octahedral $^{(6)}Al(OH)_3$, tetrahedral $^{(4)}SiO_2$, H_2O, etc. ([40] Table 2), with uncertainties ranging from 4.6 to 35.6 kJ·mol^{-1}:

Table 3
Data for calculating Dulong-Petit and modified Kopp rule estimates of Cp°_{298} values.

Site, moiety	m	Moiety bulk formula	Cp_i J·mol^{-1}·K^{-1}
DU, T	13	$Ca_2Si_2O_7H_2$	199.56
BT, S	5	SiO_3H	64.82
BT, C	4	CaO_2H	62.65
BT, v	2	OH	20.98
IC, C	6	CaO_2H_3	77.77
IC, v	1	H	7.56
IW, h	3	H_2O	28.54
BT, N	2	NaO	39.61
BT, K	2	KO	42.2
IC, N	4	$NaOH_2$	54.73
IC, K	4	KOH_2	57.32
BT, A	9	$Al(OH)_4$	101.99
IC, A	8	$AlH(OH)_3$	88.57
IC, F	8	$FeH(OH)_3$	99.58

For sublattice sites and moieties, see Table 1. The Cp_i values, used in Eq. (6), were calculated using the element contributions taken from ([39], Table 1); m is the number of element atoms per formula unit, used in Dulong-Petit rule estimates Eq. (5).

Table 4
Estimates of standard molar volumes, absolute entropies and heat capacities of CASH+ core model endmembers at $T = 25$ °C (298.15 K), $P = 1$ bar (0.1 MPa).

Name	V°_{298} cm^3·mol^{-1}	V_m nm^3/fun	S°_{298} VBT J·mol^{-1}·K^{-1}	Cp°_{298} VBT J·mol^{-1}·K^{-1}	Cp°_{298} m.K. J·mol^{-1}·K^{-1}	ΔCp°_{298} VBT-m.K.
TSvh	**138.6**	0.2301	**369.4**	**348.1**	300.5	47.6
TSCh	**155.8**	0.2586	**414.4**	**389.9**	370.7	19.2
Tvvh	**106.1**	0.1761	**284.1**	**269.0**	256.6	12.4
TCvh	**126.8**	0.2106	**338.6**	**319.6**	298.3	21.3
TvCh	**133.5**	0.2217	**356.1**	**335.8**	326.9	8.90
TCCh	**154.3**	0.2562	**410.5**	**386.3**	368.5	17.8

Values of density set to $d = 2.5$ g·cm^{-3} for TSvh and $d = 2.7$ g·cm^{-3} for all other endmembers, with 4% (0.1 g·cm^{-3}) uncertainty. Values of S°_{298} calculated from VBT Eq. (3), with 10% uncertainty. Values of Cp°_{298} obtained from VBT Eq. (4), with 30% uncertainty. "fun" stands for the formula unit; "m.K." for the modified Kopp method (Eq. (6)); "VBT-m.K." - for the difference of values obtained using VBT Eq. (4) and modified Kopp Eq. (6). CASH+ endmembers with names and values shown in a boldface black font form the "core" model and were not adjusted in model parameterization variants.

$$G^{*}_{298} = \sum_i n_i g_i \tag{7}$$

$$H^{*}_{298} = \sum_i n_i h_i \tag{8}$$

where n_i is the number of moles of i-th polyhedral component per mole of the mineral. Chermak and Rimstidt [40] commented that, even though one can calculate the estimate of standard absolute entropy S^{*}_{298} out of the estimates given by Eqs. (7) and (8), such an entropy estimate would be much less accurate than that obtained from correlations with molar volume, such as suggested by Holland [41] (which evolved into VBT methods [31] later on).

In trial calculations, we have found that the polyhedral units $^{(4)}SiO_2$, $^{(6)}CaO$, H_2O, $^{(6-8)}Na_2O$, $^{(8-12)}K_2O$, $^{(6)}Al(OH)_3$ could be assigned to all sites except IC sites, where the best results were obtained using $^{(8\text{-}z)}CaO$, $^{(6)}Al(OH)_3$, $^{(6-8)}Na_2O$, $^{(8-12)}K_2O$ units. Table 5 shows a comparison of G^{*}_{298} and H^{*}_{298} estimates obtained from Eqs. (7) and (8) with such estimates derived from the reactions with $\Delta_r G^{*}_{298} = 0$ and $\Delta_r H^{*}_{298} = 0$ involving the T5C, T2C and TobH endmembers from CSH3T model ([4], Tables 7, 8). As seen in Table 5, the polyhedral contributions "pc"-estimated values of G^{*}_{298} and H^{*}_{298} deviate not more than 50 kJ·mol^{-1} or 1% of the value (normally much less) from the "re" (reaction-estimated) values. This is at the lower end of uncertainties 1% to 3% (typically 1.5%) associated with calorimetry measurements [42].

Conversely, in the absence of reliable analogues of CASH+ endmembers, the "polyhedral contributions" values of G^{*}_{298} can be assumed to have the intrinsic uncertainty $\delta G^{*}_{298} < 50$ kJ·mol^{-1} (deduced from Table 5) and can be used as feasible initial estimates for GEMSFITS parameterization using global optimization algorithms [29]. The estimated H^{*}_{298}(pc) values are also consistent with H^{*}_{298}(re) values computed from the G^{*}_{298}(re) values and VBT-estimated S^{*}_{298} values from Table 4: as seen in Table 5, the differences $\Delta H^{*}_{298} = H^{*}_{298}$(pc) − H^{*}_{298}(re) are within −8.2 and 41.0 kJ·mol^{-1}, or within less than 1% uncertainty interval. This means that a combination of VBT, polyhedral contributions, and exchange reaction prediction methods can yield consistent estimates of all standard molar properties for all Ca-Si-H_2O sub-system endmembers.

2.5. Thermodynamics of mixing in a sublattice solid solution

A collection of endmember substances with pure-state standard molar thermodynamic properties, such as that constructed in previous sections, is only the first step to use the solid solution of variable composition in calculations of multi-phase chemical equilibria. The endmembers have to be combined into a k-th phase (-solution) definition. The bulk elemental composition of the solution phase, expressed in mole amounts of N_k chemical elements n_i, $i = 1 \ldots N_k$, can alternatively be given in mole amounts of L_k endmembers n_j, $j = 1 \ldots L_k$. Concentrations of endmembers in solid solutions are usually considered in mole fractions $x_j = \sum_j n_j$.

Substitutions in an s-th structural site (sublattice) occur via replacement of chemical moieties (atoms, ions, etc.) indexed with m, so the current composition of the s-th sublattice can be expressed via the site fractions $^{s}y_m$ of all moieties that can occur in s-th sublattice. If there is only one sublattice with substituting moieties, as in e.g. (Ba,Sr,Ra)SO_4 solid solution where cations mix randomly in one cationic sublattice, and the anionic sublattice is always occupied with sulphate ions, then there are as many endmembers as the substituting moieties, and mole fractions of endmembers x_j are equal to the respective site fractions $^{1}y_m$ of end-member-forming moieties and $j = m$. If there are two or more sublattices with substitutions then these relationships become more complex, as described in Appendix A1 (see Supporting Material).

In the current section, we only provide some general remarks necessary for understanding the CASH+ model non-ideal mixing and its parameterization. We tried two variants of sublattice solid solution models available in GEMS codes: Berman and CEF (compound energy formalism), see Appendix A1, that are based on the same sublattice solution concept, but differ in some aspects of setting up the endmembers and in the structure of non-ideal interaction parameters. Both models include reciprocal Gibbs energy contributions (optional in Berman model).

The total Gibbs energy per mole of a solid solution phase (minimal in equilibrium) is defined as

$$G_k = \sum_j x_j \mu_j = \sum_j n_j \mu_j \Big/ \sum_j n_j \tag{9}$$

Table 5
Initial estimates of G^{*}_{298} and H^{*}_{298} of Ca-Si-H_2O endmembers of the CASH+ model at $T = 25$ °C (298.15 K), $P = 1$ bar (0.1 MPa).

Name	G^{*}_{298} from reaction	G^{*}_{298}(re) kJ·mol^{-1}	G^{*}_{298}(pc) kJ·mol^{-1}	ΔG^{*}_{298} pc-re	H^{*}_{298}(re) J·mol^{-1}·K^{-1}	H^{*}_{298}(pc) J·mol^{-1}·K^{-1}	ΔH^{*}_{298}(pc-re)
TSvh	2TobH = TSvh + 2H_2O	**−4648.70**	−4619.84	28.86	−5033.47	−5003.32	30.15
TSCh	2.4T5C = TSCh + 2H_2O	**−5570.42**	−5569.83	0.59	−6054.30	−6031.73	22.57
Tvvh	TSvh = Tvvh + $SiO_{2(am)}$	**−3770.93**	−3765.89	5.04	−4114.37	−4092.35	22.02
TCvh	2T2C = TCvh + 2H_2O	**−4459.85**	−4435.02	24.83	−4830.02	−4789.00	41.02
TvCh	TCvh + H_2O = TvCh	**−4688.16**	−4715.88	−27.72	−5122.65	−5120.76	1.89
TCCh	TCvh + $Ca(OH)_{2(cr)}$ = TCCh	**−5347.99**	−5385.01	−37.02	−5809.24	−5817.41	−8.17

Standard properties of $Ca(OH)_{2(cr)}$ and $SiO_{2(am)}$ taken from GEMS PSI Nagra 07 and Cemdata 18 databases, respectively. Standard properties of liquid H_2O taken from [43]. The values of G^{*}_{298}(re) calculated from indicated reactions with $\Delta_r G^{*}_{298} = 0$. The value of H^{*}_{298}(re) calculated from G^{*}_{298}(re) and S^{*}_{298} VBT-predicted value given in Table 3. G^{*}_{298}(pc) from Eq. (7), H^{*}_{298}(pc) from Eq. (8). The G^{*}_{298} values taken as initial for the GEMSFITS parameterization are shown in boldface.

where μ_j stands for the chemical potential of j-th endmember. The complete form of μ_j as used in sublattice solution models is

$$\mu_j = \mu_j^o + RT\left(lnx_j + ln\lambda_j + lnf_j + ln\gamma_j\right) \quad (10)$$

where $\mu^o_j = G^o_j$ is the standard state chemical potential (Gibbs energy per mole) of the pure endmember j; f_j is the activity coefficient related to the excess Gibbs energy of mixing:

$$G_k^{EX} = RT\sum_j x_j lnf_j \quad (11)$$

λ_j and γ_j are fictive activity coefficient terms related to the configurational entropy of mixing on sublattices [44] and the reciprocal energy term [45], respectively (more in Appendix A1). Both λ_j and f_j are unities in the case of a simple single-site mixing such as in (Ba,Sr,Ra)SO_4 solid solution. The reciprocal term $\gamma_j = 1$ only if the Gibbs energy effects of all possible reciprocal reactions between endmembers equal zero.

In the CEF approach [46,47], the total Gibbs energy per mole of k-th phase is represented as

$$G_k = G_k^{ref} - TS_{k,id}^{conf} + G_k^{EX} \quad (12)$$

where $G_k = \sum_j \mu_j x_j$; $S^{conf}_{k,id}$ is the configurational entropy term (see [44]); $G^{EX}{}_k$ has a different form compared with Berman model; and $G^{ref}{}_k$ is the so-called frame-of-reference Gibbs energy that includes all endmember- and reciprocal contributions.

For substitutions in one sublattice only, $G_k^{ref} = \sum_{m_1} y_{m_1} G^o_{m_1}$ where $G^o_{m_1} = \sum_j x_j G^o_j$.

For simultaneous substitutions in two sublattices, $G_k^{ref} = \sum_{m_1}\sum_{m_2} y_{m_1} y_{m_2} G^o_{m_1 m_2}$, where $G^o{}_{m_1 m_2}$ is the standard-state Gibbs energy of pure end-member made of a moiety m_1 in sublattice #1 and moiety m_2 in sublattice #2. For three sublattices (as in the complete CASH+ model, Table 1), $G_k^{ref} = \sum_{m_1}\sum_{m_2}\sum_{m_3} y_{m_1} y_{m_2} y_{m_3} G^o_{m_1 m_2 m_3}$, where each pure endmember is made of a moiety m_1 in sublattice #1, moiety m_2 in sublattice #2, and moiety m_3 in sublattice #3. Complex relationships between mole fractions of endmembers x_j and moiety site fractions $^s y_m$ in the general case are described in Appendix A1 and references therein.

2.6. Possible cases of non-ideal mixing on sublattice sites

Because it was not known in advance what sublattice solid solution model variant (Berman or CEF) works better in the CASH+ model when compared with the experimental data, we have summarized in Table 6 their common or different features, as implemented in GEMS codes.

Clearly, regarding the types of interactions and the number of interaction parameters, the Berman model can be much less complex than the CEF model. Consider the (A,B,C):(L,M): solid solution with two sublattices (such as the CASH+ core model). In the Berman model, four symmetric interaction parameters $^sW_{ij}$ (three between moieties in the first sublattice, $^1W_{AB}$, $^1W_{AC}$, $^1W_{BC}$, and one in the second sublattice, $^2W_{LM}$) or 9 asymmetric ones $^sW_{ijk}$, ($^1W_{AAB}$, $^1W_{ABB}$, $^1W_{AAC}$, $^1W_{ACC}$, $^1W_{BBC}$, $^1W_{BCC}$, $^1W_{ABC}$, $^2W_{LLM}$, $^2W_{LMM}$) are possible. A Berman interaction parameter defines the interaction between moieties on a given sublattice only, regardless of what moieties occupy other sublattice(s). In the CEF model [46,47], twelve symmetric (regular) interaction parameters are possible even in the simplest case. A CEF interaction parameter accounts for the interaction energy between two moieties on a sublattice site when other sites are fully occupied each with one of their moieties.

In a sublattice solid solution, the reciprocity (described in Appendix A1) means that some endmembers and their standard thermodynamic properties can be defined via the others. In the (A,B,C):(L,M): example, six endmembers are possible: A:L:, B:L:, C:L:, A:M:, B:M:, C:M:. Three exchange reactions can be written between these endmembers:

A:L: + B:M: = A:M: + B:L:;

Table 6
Main features of Berman and CEF solid solution model implementation in GEMS, compared.

Feature	Berman model	CEF model
Sublattices	1 to 5	1 to 5
Moieties	Any number per sublattice	Any number per sublattice
Endmembers	1 to 3 moieties per sublattice (partial occupancy)	1 moiety per sublattice (single occupancy)
Reciprocity	Optional (when all possible endmembers with single-occupancy in all sublattices are present)	Required (all possible endmembers must be present in the solid solution phase)
Non-ideal mixing in sublattices	Symmetric (pairwise between moieties entering a given sublattice, regardless of moieties occupying other sublattice(s)) with interaction parameters $^sW_{ij}$ Asymmetric (between two or three moieties on sublattice) with interaction parameters $^sW_{ijk}$ when $i = j \neq k$ or $i \neq j = k$ or $i \neq j \neq k$. Temperature-pressure dependence: $W = a - bT + cP$	Symmetric (pairwise between moieties entering a given sublattice depending on which moieties are occupying other sublattices) with interaction parameters $L_{ij:k:m}$, $L_{i:kl:m}$, $L_{i:k:mn}$, $L_{ij:kl:m}$, … where the maximum number of indices is twice the number of sublattices, and permutation goes over all moieties entering each sublattice. Temperature-pressure dependence: $L_{IZ} = a + bT + c\ln T + dP$

B:L: + C:M: = B:M: + C:L:;

A:L: + C:M: = A:M: + C:L:

Each reaction has its own standard Gibbs energy effect, which can be non-zero and thus result in reciprocal contributions to chemical potentials of endmembers that depict a special kind of non-ideality of mixing. In Berman model implementation, reciprocal terms are optional, but they should be taken into account if the reciprocity is present indeed (as in the CASH+ model).

2.7. Thermodynamic system, databases, and software

Due to complexity of sublattice solid solution models, with many parameters to be adjusted at the same time, we used the GEM-Selektor and GEMS3K codes [48] with the TSolMod library of solution models [49] and the GEMSFITS code [29] for the CASH+ model multiple parameter optimization following a stepwise fitting strategy outlined below. Thermodynamic data for other phases except C-S-H were taken from the PSI/Nagra 12/07 [28] and Cemdata18 [27] chemical thermodynamic databases. Activity coefficients of aqueous species were computed using the extended Debye-Hückel equation [50]:

$$log\gamma = \frac{-Az_j^2\sqrt{I}}{1 + \mathring{a}B\sqrt{I}} + b_\gamma I \quad (13)$$

where A and B represent the Debye-Hückel solvent parameters, $\mathring{a}$ is the common ion size parameter, b_γ is an extended term parameter, and I is the effective ionic strength. Values for $\mathring{a} = 3.67$ Å and for $b_\gamma = 0.123$ as for KOH as major electrolyte are used in modelling cement systems using Eq (13). Activity coefficients of neutral aqueous species and water were calculated as coded in the model implementation in TSolMod library [49].

3. Initial parameterization for Ca-Si-H_2O core part of CASH+ model

The new structurally plausible CASH+ sublattice solid solution model, constructed using alternatively the non-ideal Berman sublattice model [51] or the Compound Energy Formalism (CEF) [16,46], with thermodynamic properties computed using GEMS codes, is expected to be accurate and flexible. To demonstrate and validate this expectation,

the model must be properly parameterized by fitting its parameters against the available experimental solubility and spectroscopy data.

The difficulties in such fitting exercises, apart from the expertise needed for compilation of the experimental data, consist in that most endmembers generated in a sublattice solid solution model do not exist in pure state, and the mixing part of the model may have many site interaction parameters. This necessitates (i) the systematic prediction of initial standard thermodynamic properties of endmembers from their composition (as described in previous sections), and (ii) the usage of an advanced multi-parameter optimization tool such as the GEMSFITS code [29].

In the next sections, we describe the initial parameterisation of the Ca-Si-H_2O core part of the CASH+ model. The incremental extension with end-members containing alkali and alkali earth cations and involving new experimental data sets will be reported elsewhere [24], as well as the extensions with aluminum- and iron(III) containing end-members [25] and hazardous cations [26]. We had to split the results in this way because to include everything in one paper would really inflate it to a full book size.

3.1. Selection of experimental data

For the CASH+ model parameterization in the Ca-Si-H_2O sub-system, we used several experimental datasets listed in Table 7. Walker et al. [2] put together an extensive critical compilation of almost all C-S-H solubility data available to date. We used a selection of these data for C3S hydration and for co-precipitation or double decomposition experiments. For the parameter refinement process, we used the measured aqueous phase total elemental concentration ($[Ca]_{aq}$, $[Si]_{aq}$) and reported C/S ratio in C-S-H phase (Table 7).

To improve the structural consistency of the sublattice solid solution model of C-S-H, the MCL data had to be included in the fitting at some stage. However, the ^{29}Si MAS NMR data, from which the MCL data was derived, are scarce and not available for all samples in all datasets. Fortunately, for some of the measurements in [52–55], the authors reported the MCL data, which follow the same trend as function of C/S ratio in C-S-H for all three co-precipitation datasets (Fig. 3). Because the MCL data resulting from the deconvolution of ^{29}Si MAS NMR are associated with a considerable inaccuracy and are less abundant than the solubility data, the available MCL data in these three datasets was regressed using an exponential decay function

$$MCL = (0.391 \pm 0.083) exp \frac{(2.302 \pm 0.267)}{C/S - (0.195 \pm 0.035)} \quad (14)$$

where C/S stands for the C/S ratio in C-S-H. This function that fits the measured MCL data quite well, was subsequently used to fill out the MCL data gaps (as a function of C/S) in all three experimental datasets. Eq. (14) produces a curve shape similar to that obtained from the relation suggested in [23]:

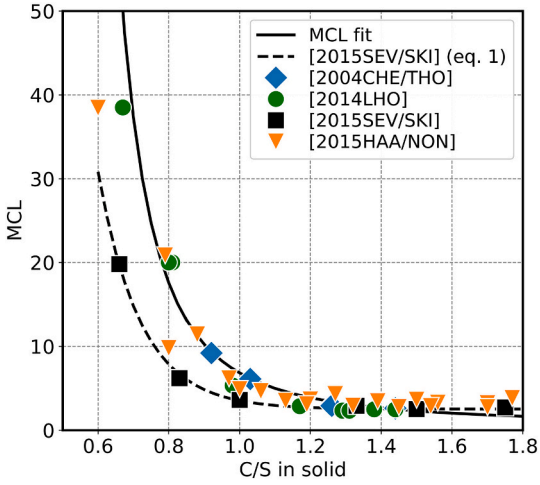

Fig. 3. MCL data plotted against C/S ratio in C-S-H. MCL-fit is the curve of Eq. (14). Data sources: [2004CHE/THO]: [52]; [2014LHO]: [53,54]; [2015HAA/NON]: [55] (and PhD theses by E.L'Hopital and J. Haas); [2015SEV/SKI] [23].

$$MCL = a \cdot exp\left(- C/S^{\cdot 1}/b \right) + c \quad (15)$$

where $a = 4206$, $b = 0.12$ and $c = 2.5$. The "regressed" MCL pseudo-data was used together with the compositional data in the parameter fitting. Reported and generated MCL data was only used in the optimization process for the datasets from [52–55].

3.2. Model parameterization approach

The following strategy has been developed for the stepwise parameterization of the CASH+ model at pressure 1 bar and ambient temperatures 20, 23 or 25 °C.

(1) Begin the optimisation with the Ca-Si-H_2O sub-system (initial G^*_{298}(re) of 6 endmembers from Table 5, other (estimated) standard properties from Table 4) using or not the reciprocal terms γ_j, and with all zero interaction parameters W or L.
(2) Proceed with keeping G°_{298} values of endmembers at values obtained at Step (1) while optimizing 4 (symmetric Berman) interaction parameters W.
(3) Proceed with optimizing G°_{298} values of endmembers simultaneously with interaction parameters W, starting from the values obtained at Step (2), against both the C-S-H solubility and the regressed MCL pseudo-data (Fig. 3, Eq. (14)).
(4) Proceed with the simultaneous fitting of G°_{298} values of endmembers, interaction parameters W, and G°_{298} value of the $CaSiO_3^0$ aqueous complex against both C-S-H solubility and MCL pseudo-data.

Table 7
Selected experimental datasets for parameterization of the C-S-H subsystem.

Reference	Code in figures	Type, s/w mass ratio	Starting materials	Equilibration time (month)	Temperature (°C)	Target C/S ratio
[52][a]	[2004CHE/THO]	DD, C3S >50	$Ca(NO_3)_2$ and Na_2SiO_3	8	22	0.1–2.0
[53]	[2014LHO]	DR (CP) 45	CaO and SiO_2	3–18	20	0.6–1.5
[55]	[2015HAA/NON] [2012HAA]	DR (CP) 50	CaO and SiO_2	>1	25	0.64–1.66
[56]	[2016SWA/HEA]	DR (CP) 150	CaO and SiO_2	1–12	25	0.2–0.6
[57]	[2015ROO]	DR (CP) 50	CaO and SiO_2	1	22	0.2–1.6
[58]	[2014PLU]	DR (CP) 20	CaO and SiO_2	1	23	0.8–1.2
[59][a]	[2005HEN]	DR, C3S 50	CaO and SiO_2	0.75	25	0.7–2.5
[60]	[2007WAL/SAV]	DR, 10	CaO and SiO_2	6	20–25	0.8–2

[a] Experimental data on C3S hydration were also reported, but not used in the fit. DD: double decomposition; DR: direct reaction; CP: co-precipitation experiments. The solid/water (s/w) ratios are given in g(CaO + SiO_2)/kg(water).

(5) Fine-tune the CASH+ model by adding more experimental data from Walker et al. [2] compilation and by assigning weights to experiments such that the C-S-H phase would have C/S = 1.65 at the appearance of portlandite.
(6) Keep all parameters that were fitted up to this step fixed in further extensions of the CASH+ model. Verify CASH+ solid solution core model parameterized at steps 4 and 5 in forward modelling of C-S-H composition, solubility, and density in various systems.

3.3. CASH+ core model parameterization results

At Step 1, we tested whether an ideal sublattice solid solution model (with- or without reciprocal terms, but with zero interaction parameters) would be sufficient to describe the experimental data. Six initial G^*_{298}(re) values for endmembers (Table 5) were adjusted using global algorithms and allowing ±50 kJ·mol^{-1} upper and lower bounds and different weights on measured data: (a) equal weight of 1 for the aqueous and solid phase composition and MCL; (b) a weight of 1 for the composition and a larger weight of 5 for the MCL; (c) a weight of 1 for the composition and a smaller weight of 0.1 for the MCL.

In all cases, the fits with reciprocal terms were better than without them. Using the model with reciprocal terms, we were able to fit the G°_{298} values for 6 endmembers and get a satisfactory representation of the solubility data (Fig. 4, Step 1), though somewhat worse in the interval 0.9 < C/S < 1.2. However, it was not possible to accurately reproduce measured aqueous and solid composition and MCL pseudo-data at the same time, regardless of weights.

At Step 2, the symmetric Berman interaction parameters (see Section 2.6) were added to the fitting task: one parameter for IC sublattice, and three for BT sublattice. The fits were first run for interaction parameters only, while keeping G°_{298} values fixed from Step 1. We assigned the ±50 kJ·mol^{-1} upper- and lower bounds for interaction parameters and equal weight of 1 to the different types of measured data (used also in the following steps). However, this did not lead to the desired improvement of the overall fit to the solubility data.

At Step 3, all ten parameters (i.e. six G°_{298} values for endmembers plus four $^sW_{ij}$ values for interaction parameters) were adjusted simultaneously. We assigned upper and lower bounds of ±30 kJ·mol^{-1} for G°_{298} of endmembers and ± 10 kJ·mol^{-1} for the interaction parameters. The resulting fit reproduces both the input solubility data and the MCL pseudo-data (Fig. 4, step 3). At steps 1 to 3, no adjustment was done on G°_{298} of $CaSiO_3^0$ complex. For steps 1 to 3, we used its properties as reported in Nicoleau and Schreiner [61], and the measured dissolved silica was always underpredicted by the model (Fig. 4 A). However, by scoping calculations, we have found (in tune with conclusions in Walker et al. [2]) that modelled dissolved $[Si]_{aq}$ at C/S > 1.3 was very sensitive to G°_{298} value of $CaSiO_3^0$ complex.

At Step 4, we tested the influence of the stability of $CaSiO_3^0$ complex on parameterization of the C-S-H model. For that, we added the G°_{298} of $CaSiO_3^0$ as one more fitting parameter (to the 10 other parameters considered in step 3) with upper and lower bounds of ±10 kJ·mol^{-1}. No fitting for $CaHSiO_3^+$ complex was attempted, as this complex was very minor in the whole C/S range (Fig. 5, C). We obtained a better agreement between the measured and the calculated aqueous solubilities (Fig. 4, step 4), with 25% less the sum of squared residuals for the measured and calculated $[Si]_{aq}$ values. The refined G°_{298} value of $CaSiO_3^0$ was −1514.14 kJ·mol^{-1}, corresponding to $\log K^\circ_{298}$ = 4.0 for the reaction $Ca^{2+} + SiO_3^{2-} = CaSiO_3^0$. This fitted value is nearly identical to that proposed in [2], meaning that the $CaSiO_3^0$ complex is 0.6 pK units less stable than the value given in the PSI-Nagra database 12/07 and 1.1 pK units more stable than the value suggested by Nicoleau and Schreiner [61]. The results of fitting at Step 4 are given in Table A1-4 in the Supplementary Material.

In steps 1 to 4, only three datasets [52–55] were used in the fitting, while in step 5, we added all other datasets reported in Table 7 to the optimization process. During the optimization procedure, we also constrained the C/S ratio in C-S-H in equilibrium with portlandite close to 1.65. This value corresponds to the typical C/S in CSH co-existing with portlandite in samples obtained by C_3S hydration, as reported in [2] based on their review of a large selection of experimental data.

To better constrain the parameters in step 5, we took their values from step 4 as initial values. We have selected the experimental datasets suggested in the critical review by Walker et al. [2]. In addition to the optimized values, 95% confidence intervals for the fitted parameters were retrieved at Steps 4 and 5 using the Monte Carlo (MC) method as implemented in GEMSFITS code (details in Miron et al. [29] and Appendix B1 in Supporting Material).

Fig. 5 shows the comparison of calculated and measured experimental data, as well as the modelled composition of solid C-S-H and aqueous solution phases using the final set of parameters obtained in step 5 (Table 8) with increasing C/S in the solid. In Fig. 5, A we compared the calculated total aqueous concentrations $[Si]_{aq}$ and $[Ca]_{aq}$ with their measured counterparts from the extended experimental dataset that was used at step 5. Fig. 5, B shows the mole fraction of each CASH+ core end-member for the same C/S interval as in Fig. 5, A. C-S-H is the only phase present in the system between C/S 0.72 and 1.65 with amorphous silica SH and portlandite CH phases stable at low and high C/S ratios, respectively. Mole fractions of endmembers (Fig. 5, B) are given only for illustrative purposes because, as shown in Appendix A1.4, their variations along the C/S axis depend on the type of GEM automatic

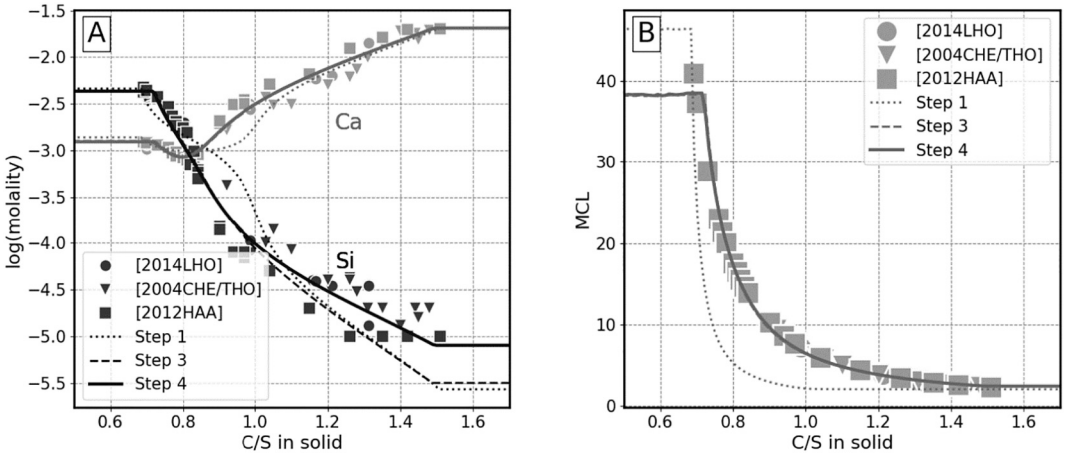

Fig. 4. CASH+ core sub-model comparison between measured and calculated values for A: Solubility of C-S-H; B: MCL as a function of bulk C/S ratio, symbols are pseudo-data from Eq. (14). Experimental data points from [53,54], [52], and [55]. Computed with the GEM-Selektor code v.3.7 using thermodynamic data for CASH+ endmembers from Tables 4 and 9.

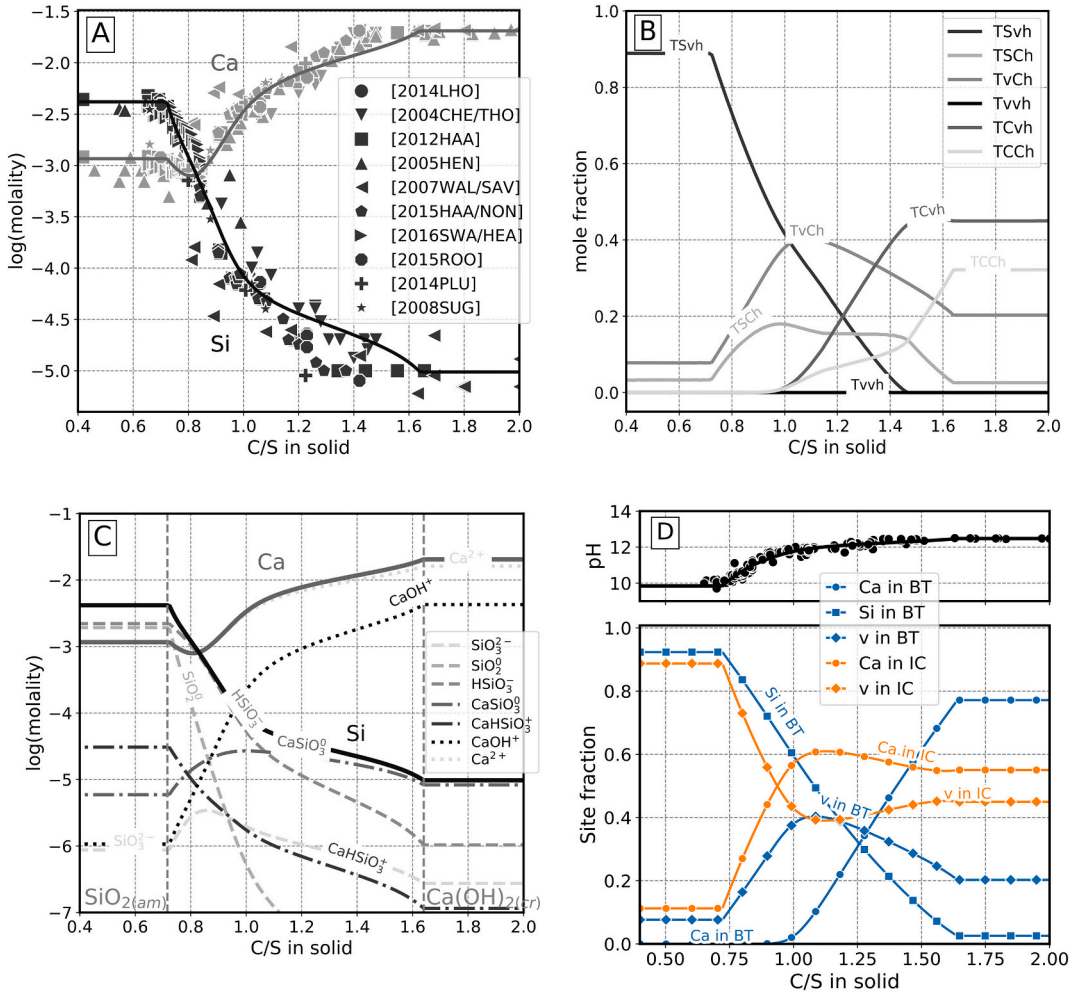

Fig. 5. Modelled C-S-H system with increasing target C/S using the final fitted set of parameters (Table 10). (A) comparison of measured (see Table 7) and calculated $[Ca]_{aq}$ and $[Si]_{aq}$ concentration; (B) mole fraction of endmembers at the same conditions as in A; (C) aqueous speciation, the sum of Si and Ca species (dashed lines) give the concentration of Si and Ca in the aqueous solution; (D) site fractions. Until ~0.71 target C/S, amorphous silica $SiO_{2(am)}$ phase is stable. At target C/S > 1.65, portlandite CH, $Ca(OH)_{2(cr)}$ phase is stable.

initial guess for each endmember ('M' major or 'J' junior).

The selected types, shown in Table 8, result in a best-interpretable model behaviour (where Tvvh endmember is suppressed in the whole C/S range). Other plots (site fractions, $[Ca]_{aq}$, $[Si]_{aq}$, pH etc.) come out the same regardless of the initial guess choices for endmembers. This behaviour is the consequence of the reciprocity in the sublattice solid solution, where less endmembers are needed to describe the bulk properties than to describe the mixing behaviour (more in Appendix A1). Fig. 5, C shows the Si and Ca aqueous solution speciation. There is a notably different speciation for two elements, and in the case of silica, it changes dramatically at different target C/S ratios.

The total aqueous dissolved calcium $[Ca]_{aq}$ is dominated by the calcium ion, Ca^{2+}, over the whole considered C/S interval, while the total dissolved silica $[Si]_{aq}$ is described at different C/S intervals by various species. Up to C/S = 0.72, the amorphous silica SH is stable. This phase constrains $[Si]_{aq}$ that below C/S = 0.72 is dominated by SiO_2^0 and $HSiO_3^-$ species with almost equal contribution. Fig. 5, D shows the site fraction distribution in CASH+ model at different C/S. From the point where amorphous silica is no more stable with increasing C/S, a decrease of Si moiety fraction in BT sites is observed, with increase of vacancies fraction until C/S = 1 when Ca moiety starts outcompeting the vacancies. For the IC sites, we see a drop in the fraction of vacancies that are replaced by Ca, with a slight increase in vacancies above C/S = 1.1. When portlandite becomes stable, the site fractions stop changing and the C-S-H composition is fixed. Above C/S = 1.64, BT sites are mostly occupied by Ca (with site fraction of 77%), followed by vacancy (20%) and Si (3%); IC sites are occupied with Ca (55%) and vacancies (45%).

3.4. Density and water content in C-S-H

The density and water content of C-S-H gel-like phases has long been a matter of debate [32,35–37], although the recent data provide somewhat better constraints [33]. To some extent, this debate was a matter of definition: should "gel pores" be included into C-S-H composition and accounted for in density? At what relative humidity and temperature to measure densities? In this study, we assumed to exclude the "gel pore water" from composition of C-S-H, but to include the interlayer water in presence of liquid water, as corroborated from TGA, ^{1}H NMR, and water sorption isotherm data (Fig. 6, A).

The water content, expressed in H/S (H_2O/Si) mole ratios, is defined in the CASH+ model by the moiety- and endmember stoichiometry (see Section 2.3). However, the density of C-S-H as function of C/S ratio is an independent property that can be determined from neutron-scattering, ^{1}H NMR, or X-ray studies ([33] and refs therein). We have made an early-stage assumption that the density equals $d = 2.5$ g·cm^{-3} for TSvh endmember and $d = 2.7$ g·cm^{-3} for all other endmembers of the CASH+ model, with 4% (0.1 g·cm^{-3}) uncertainty. This was necessary in order to be able to compute molar volumes of endmembers, to apply the VBT

Table 8
Optimized values for Gibbs energy of formation (G°_{298}) of endmembers and symmetric interaction parameters together with 95% confidence intervals (Step 5).

Endmembers	Initial guess type	Final value (step 5)	MC confid. interv. 95%	Step 5 – step 4	Standard enthalpy[a]
		G°_{298} (kJ·mol^{-1})	δG°_{298}, δW (kJ·mol^{-1})	ΔG°_{298} (kJ·mol^{-1})	H°_{298} (kJ·mol^{-1})
TCCh	M	**−5347.54**	2.88	−4.65	−5808.79
TCvh	M	**−4450.98**	1.27	−3.07	−4821.14
TSCh	J	**−5561.94**	0.77	−1.48	−6045.81
TSvh	M	**−4647.54**	0.59	−1.29	−5032.03
TvCh	M	**−4684.56**	1.30	−5.08	−5119.05
Tvvh	J	**−3777.08**	0.58	+2.02	−4120.51

Interaction parameters[b]	W (kJ·mol^{-1})	δW (kJ·mol^{-1})	W_{init}
$^{IC}W_{Cv}$	**−17.12**	1.76	−0.22
$^{BT}W_{Sv}$	**−19.07**	0.54	−2.98
$^{BT}W_{CS}$	**−8.56**	1.81	+9.18
$^{BT}W_{Cv}$	**−7.87**	0.74	+4.11
Aqueous complex	G°_{298}(kJ·mol^{-1})	δG°_{298}, (kJ·mol^{-1})	ΔG°_{298}(kJ·mol^{-1})
$CaSiO_3^0$	**−1514.14**	0.24	−1.81

Other standard thermodynamic properties of endmembers are given in Table 4 (boldface). The fits performed using the data from all selected sources shown in Fig. 5. Initial values of G^{*}_{298} of endmembers taken from Table 5; in global fitting runs, initial bounds of ±50 kJ·mol^{-1} applied to G^{*}_{298} values and Berman symmetric interaction parameters $^{s}W_{ij}$; initial bounds of ±10 kJ·mol^{-1} applied to G^{*}_{298} value of the $CaSiO_3^0$ complex.

[a] Values of H_{298}° calculated using G_{298}° (Step 5) and S_{298}° from Table 4.

[b] See explanations to Table 4. Initial guess type (for an endmember): M – major; J – junior.

(volume-based thermodynamics) methods to obtain reliable estimates of standard entropy, and heat capacity of all endmembers, and to show the consistency of fitted or estimated values of standard enthalpy at ambient conditions.

Fig. 6, B shows the evolution of C-S-H (fully hydrated) density and water content as H/S ratio with the increasing target C/S ratio. At low C/S, the CASH+ core model calculates the density to be around 2.5 g·cm^{-3}; it then increases at intermediate C/S ratios to a value of 2.7 g·cm^{-3} at high C/S. The density is calculated from the mass of C-S-H phase present in equilibrium and its volume (both obtained as GEM-Selektor results). The volume is retrieved from the standard-state volume of endmembers (Table 4). The calculated H/S ratio agrees well with the available literature data [32,33,35,54,62,63]; it starts from a value of 1.07 at low C/S and goes up to H/S = 1.75 at high C/S, with the experimental points scattered around the calculated curve.

3.5. *Effect of temperature onto C-S-H properties as predicted by CASH+ core model*

Consistent values of standard molar entropy S°_{298} and heat capacity Cp°_{298} of CASH+ endmembers were estimated in Section 2.4 using the VBT equations (Table 4). Parameters for temperature corrections of standard molal properties of aqueous species and standard molar properties of minerals are available from PSI-Nagra [28] and Cemdata18 thermodynamic databases [27]. Taken together, all these parameters are expected to provide reasonable temperature trends for density, stability, composition and solubility of C-S-H at least within the 10 °C and 90 °C range. Interaction parameters in Berman model are expressed in kJ·mol^{-1} and, hence, contain an intrinsic temperature correction as $W/(RT)$, i.e. they become weaker with the increasing temperature, which is typical for most mineral solid solutions.

Instead of performing GEMSFITS parameter optimizations against the (scarce) available C-S-H solubility data at elevated temperatures, we decided to test whether a blind prediction of temperature trends is possible, just using VBT-estimated properties of CASH+ endmembers from Table 4. Below, we discuss some results of this forward modelling conducted in GEM-Selektor as temperature profiles, and try to evaluate how realistic they are.

The obvious anchor point is the composition of the system, at which the C-S-H phase co-exists in equilibrium with portlandite CH ($Ca(OH)_2$). Recent literature provides some experimental data on properties of C-S-H in Portland cement at different temperatures [33].

Fig. 7 compares some predicted temperature trends with the experimental data from that paper, where also the kinetics trend is established at 28 and 90 days of hydration. The CASH+ core model predicts constant solid density and almost constant solid H/S and C/S ratios in presence of

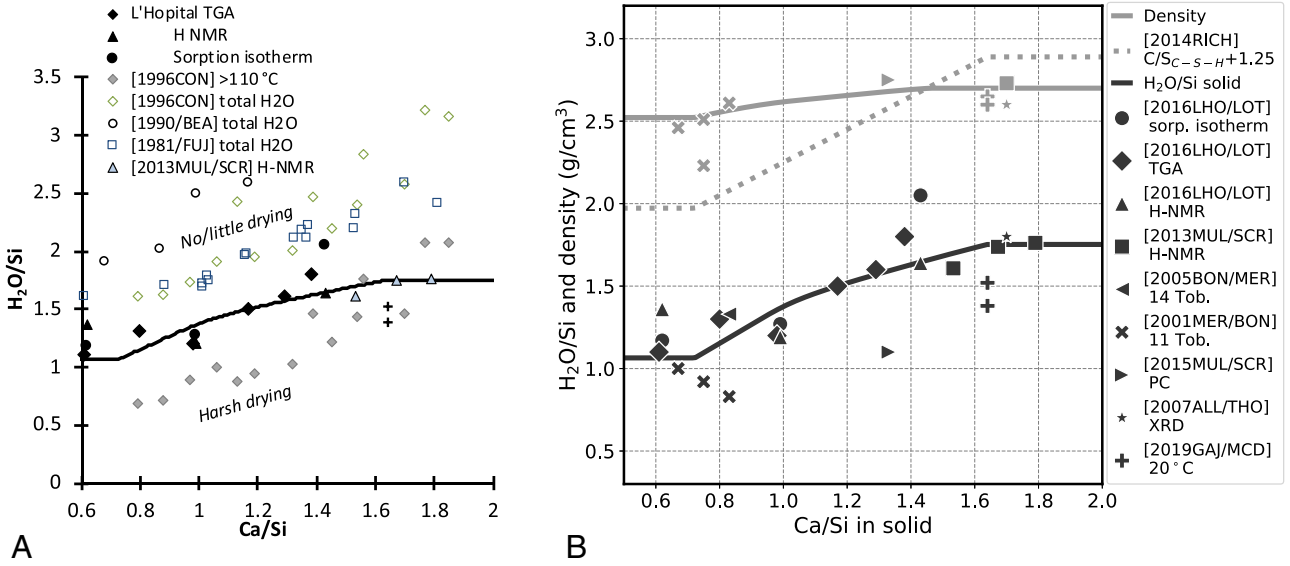

Fig. 6. CASH+ model calculated density and water content (H/S ratio, H_2O/Si) for fully hydrated C-S-H versus the increasing C/S ratio in solid, compared with the compilation of available experimental data indicated by various symbols [32,33,35,54,62,63]. (B) Calculated (curves) vs available (scatter) H/S ratios (solid) and densities (gray); the experimental and crystallographic data from [32,33,35,38,54,62,63]. Dotted curve: d_c (g·cm^{-3}) = C/S + 1.25 from [38].

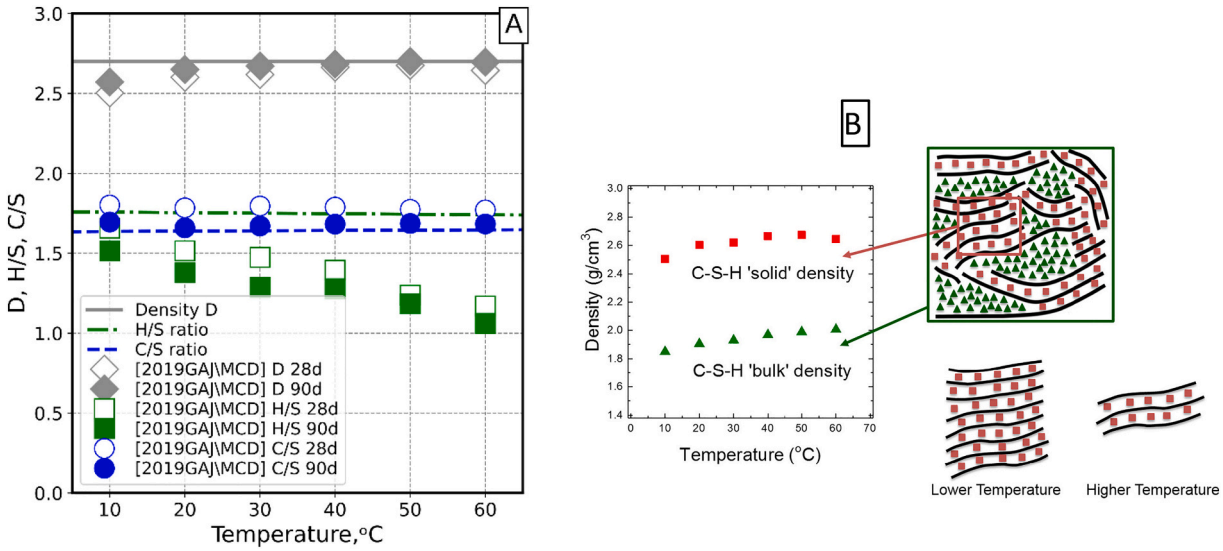

Fig. 7. A: comparison of temperature trends of density (in g·cm^{-3}), H/S and C/S ratios computed using the CASH+ core solid solution model (Table 8), lines for C-S-H in presence of portlandite, with the experimental data [2019GAJ\MCD] from [33] for OPC (28 days hydration, open symbols; 90 days hydration, closed symbols). Note a discrepancy for H/S ratio (green squares) and a good agreement for the density (gray diamonds) and C/S ratio (blue circles). B: Graphical abstract from [33], showing the relationships between solid- and gel-water contents in C-S-H at lower and higher temperatures. For interpretation of the references to colour in this figure legend, the reader is referred to the web version of this article [33].

portlandite. Except the H/S ratio (non-gel water content), the model curves describe the data for 90 days reasonably well. The calculated H/S ratios correspond to the experimental one at the lowest temperatures only, because the experimental values show a decreasing trend with increasing temperature. This is also a very basic and global trend, for most hydrates, to lose water as temperature increases or water activity decreases. The authors of [33] explain this trend by a decrease in the stacking of C-S-H platelets, from ca. 6–8 Ca-silicate layers at 10–15 °C to 3–4 layers at 50–60 °C (Fig. 8).

As their ^{1}H NMR data interpretation seems to account for H_2O confined in the interlayer, but not for H_2O sorbed on the outer basal surfaces, this may explain an apparent reduction of solid H_2O content in

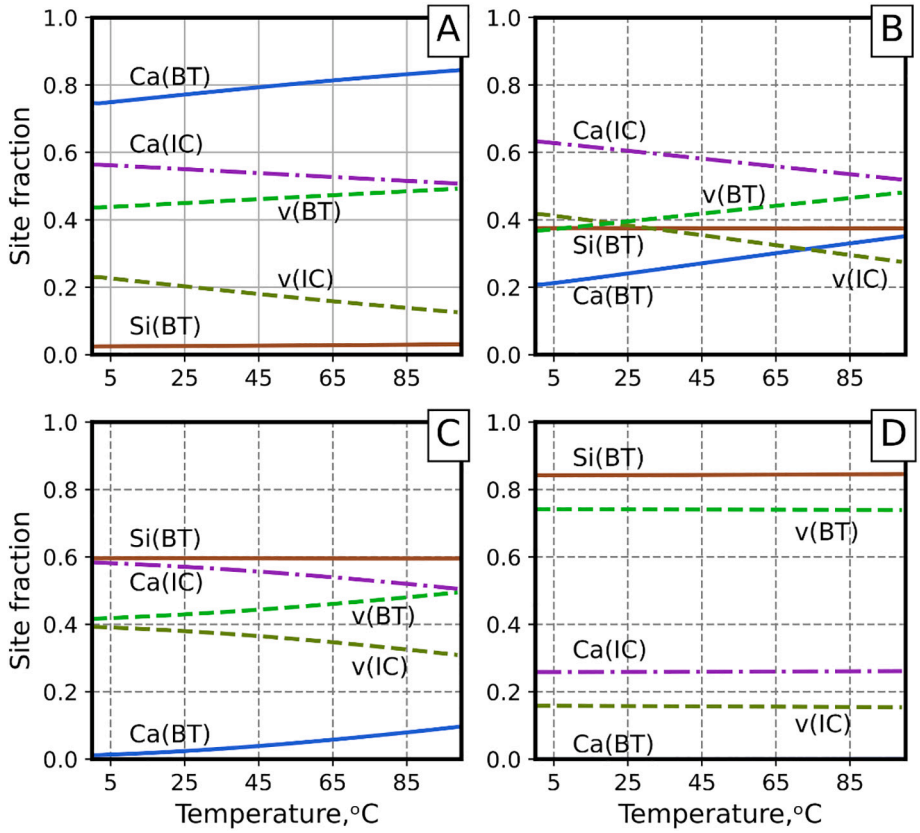

Fig. 8. Site fractions vs temperature as reproduced by the CASH+ core model: in equilibrium with portlandite at C/S > 1.63 (A); at solid C/S ≈ 1.2 (B); at C/S ≈ 1.0 (C); and at C/S ≈ 0.8 (D).

C-S-H by about 50% from 10 °C to 60 °C visible in the experimental data. The present CASH+ core model does not yet account for such effects of C-S-H particle morphology, though this may be improved in future studies by introducing new endmembers with a vacancy in the IW site (perhaps corresponding to the outer platelet surfaces), followed by the respective GEMSFITS parameterization against the temperature-dependent data.

In Fig. 8A–D, the site fractions of moieties on sublattices in the CASH+ core model at C/S > 1.6 (in equilibrium with CH), 1.2, 1.0 and 0.8 are plotted against the increasing temperature. Note the different temperature trends of site fractions in response to the different bulk compositions of C-S-H phase. Such evolution of site fractions reflects changes both in the standard Gibbs energies of endmembers and in the normalized interaction parameters. The Si in BT site fraction remains almost constant, whereas the Ca in BT site fraction steadily increases by about 10%. In IC sublattice sites, the Ca fraction decreases and becomes almost equal to vacancies fraction at temperatures around 100 °C at all C/S ratios except 0.7 (where Ca site fraction is 10% or less). The site fraction of Ca on BT sites is almost 0 at C/S = 0.8 and steadily increases to 2–9% at C/S = 1.0, 20–35% at C/S = 1.3 and 75–85% at C/S > 1.6. The site fraction of Si in BT sublattice, as expected, is high (85%) at C/S = 0.8 and decreases to about 3% at C/S > 1.6; in all cases, it shows only very little change with temperature. The case D at C/S = 0.8 shows a constancy with temperature overall; the constant site fraction of Si in BT sites also means the constant MCL, independent of T at this composition of C-S-H.

Next, the blind-prediction forward calculations of C/S profiles similar to that shown in Fig. 5, A were performed for temperatures 50 °C and 90 °C, and the model curves for $[Ca]_{aq}$, $[Si]_{aq}$ and pH were compared with a selection of experimental data from [64–67] (not shown). It turned out that the CASH+ core model (Table 8) reproduced $[Ca]_{aq}$ and pH well at all temperatures up to 90 °C without any tweaking; however, it significantly (1–2 pK units) under-predicted $[Si]_{aq}$ at higher temperatures (90 °C). From the above discussion, it follows that the $CaSiO_3^0$ complex is the main aqueous form of silica in the C-S-H - portlandite system. So, even being already fine-tuned at 25 °C, the parameters responsible for stability of $CaSiO_3^0$ at elevated temperatures need to be improved.

For estimating the temperature dependence of the $CaSiO_3^0$ complex, we initially assumed zero standard effects for molar volume, entropy and heat capacity of the reaction $Ca^{2+} + SiO_3^{2-} = CaSiO_3^0$ (the two latter silica species are taken in a "dewatered stoichiometry" as in SUPCRT98 and Nagra/PSI for GEMS databases). Involving other data from the Nagra/PSI for GEMS database leads to estimates of standard properties given in Table 9, "initial" variant.

However, it is known that temperature trends for neutral aqueous species such as SiO_2^0 or UO_2^0 can be set accurately using dissolution reactions of solids with the same stoichiometry, e.g. $SiO_{2(quartz)} = SiO_2^0$ or $UO_{2(cr)} = UO_2^0$, with standard entropy and heat capacity effects equal or close to zero for the SiO_2 reaction or log$K$ independent of T for the UO_2 reaction [84]. Therefore, we tried the approach for SiO_2^0 for defining the standard properties of $CaSiO_3^0$ using a reaction with the mineral wollastonite: $CaSiO_{3(cr)} = CaSiO_3^0$, and setting the standard volume, enthalpy and heat capacity effects of this reaction to zero. Using standard molar properties of wollastonite from [68], this resulted in estimates given in Table 9, "wollastonite" variant. These new standard properties of $CaSiO_3^0$ translate into non-zero standard effects of the reaction $Ca^{2+} + SiO_3^{2-} = CaSiO_3^0$.

Calculations of solubility of C-S-H at 50 and 90 °C yielded now a much better fit to $[Si]_{aq}$ (curves for Ca and pH almost did not change), but over-predicting most the experimental data (which are quite scattered, thus making it difficult to achieve the exact fit). Finally, the standard entropy of $CaSiO_3^0$ species was constrained to get a reasonable agreement with the C-S-H solubility data at 50 and 85–90 °C, and the heat capacity was retrieved by fitting against the quartz + wollastonite solubility experiments reported by [69] (see "accepted" values in Table 10). All three cases produce trends of log$K$ for the above reaction, shown in Fig. 9. The resulting performance of the CASH+ core model at two temperatures is shown in Fig. 10.

In Fig. 11, the temperature trends of total dissolved $[Ca]_{aq}$, $[Si]_{aq}$, and pH are shown for different solid C/S ratios in C-S-H, as predicted by the CASH+ core model (step 5, variant 5). The experimental data at 90 °C shows a large scatter for the measured dissolved $[Si]_{aq}$, having datasets that show a lower and a higher concentration. The accepted properties of $CaSiO_3^0$ make the species slightly more stable with increasing temperature, which results in a small increase of dissolved $[Si]_{aq}$ when C-S-H is in equilibrium with portlandite.

At all C/S ratios, the temperature trends of $[Ca]_{aq}$ and $[Si]_{aq}$ are almost flat. However, pH decreases about 2 to 2.5 units over a 100 degrees temperature interval. This decrease may be due to two factors: (a) decrease of pK of water dissociation reaction at higher temperatures; (2) increase of $CaOH^+$ fraction relative to Ca^{2+} at higher temperatures.

The summary of thermodynamic data for endmembers of the CASH+ core model, applicable for temperatures between 0 °C and 100 °C, is provided in Table 10.

Roosz et al. [57] produced values for entropy and heat capacity of synthesised C-S-H from calorimetric measurements. We compared their values with the values calculated using the CASH+ core model for their reported structural formulas (Table 11). The differences between $G°_{298}$ values are smaller than 2.0 kJ·mol^{-1}; the close values can be explained from the use of similar solubility data to obtain the $G°_{298}$ values.

For the $S°_{298}$ and $Cp°_{298}$, the differences do not exceed 30 J·mol^{-1}·K^{-1} and are within the acceptable uncertainty of VBT (volume-based-thermodynamics) estimates. The entropy and heat capacity values reported in Roosz et al. [57] are systematically larger than the values calculated using the CASH+ core model. This signifies that their data describe a C-S-H phase that is to some extent more stable (less soluble) with increasing temperatures than synthetic C-S-H phases used in solubility experiments, against which the CASH+ core model was fitted in our work.

3.6. Discretization of CASH+ core sublattice model for use in LMA codes

Incorporation of complex non-ideal solid solution models into reactive transport simulations is still a challenge, most probably because of missing implementation in most chemical speciation solvers. Another issue is that systems with highly non ideal solutions may behave stiff in the sense of convergence and need special smoothing procedures and, in general, more computing time. A simple, less accurate workaround in such cases is to approximate solid solution with a DSP (discrete solid

Table 9
Values of standard thermodynamic properties of $CaSiO_3^0$ complex.

Variant units	$S°_{298}$ J·(mol·K)$^{-1}$	$Cp°_{298}$ J·(mol·K)$^{-1}$	$H°_{298}$ kJ·mol^{-1}	$V°_{298}$ cm^3·mol^{-1}	$\Delta_r V°_{298}$ cm^3·mol^{-1}	$\Delta_r S°_{298}$ J·(mol·K)$^{-1}$	$\Delta_r Cp°_{298}$ J·(mol·K)$^{-1}$	$\Delta_r H°_{298}$ kJ·mol^{-1}
Initial	−136.68	88.90	−1664.6	15.69	0	0	0	−22.83*
Wollastonite	82.50	86.14	−1599.6	40.00	24.309	219.18	−2.76	42.517
Accepted	**−50**	**206.9**	−1638.8	40.00	24.309	**86.6**	**118**	**2.988**

Standard effects $\Delta_r V°_{298}$ etc. are given for the reaction $Ca^{2+} + SiO_3^{2-} = CaSiO_3^0$. *In this case, equal to $\Delta_r G°_{298}$. Recommended thermodynamic properties are shown in boldface.

Table 10
Summary of standard molar thermodynamic properties for the CASH+ core model endmembers at $T = 25$ °C (298.15 K), $P = 1$ bar (0.1 MPa).

Name	Bulk formula	d g·cm^{-3}	V°_{298} cm^3·mol^{-1}	G°_{298} J·mol^{-1}	H°_{298} J·mol^{-1}	S°_{298} J·(mol·K)$^{-1}$	Cp°_{298} J·(mol·K)$^{-1}$
TSvh	$Ca_2Si_3O_{11}H_6$	2.5	138.6	−5347.54	−5808.79	369.4	348.1
TSCh	$Ca_3Si_3O_{13}H_8$	2.7	155.8	−4450.98	−4821.14	414.4	389.9
Tvvh	$Ca_2Si_2O_9H_6$	2.7	106.1	−5561.94	−6045.81	284.1	269.0
TCvh	$Ca_3Si_2O_{10}H_6$	2.7	126.8	−4647.54	−5032.03	338.6	319.6
TvCh	$Ca_3Si_2O_{11}H_8$	2.7	133.5	−4684.56	−5119.05	356.1	335.8
TCCh	$Ca_4Si_2O_{12}H_8$	2.7	154.3	−3777.08	−4120.51	410.5	386.3

Consistent with standard molar properties of $Ca(OH)_{2(cr)}$ and $SiO_{2(am)}$ taken from GEMS PSI Nagra 07 and Cemdata 18 databases, respectively, and the accepted properties of $CaSiO_3^0$ complex from Table 9. Uncertainties of G°_{298} and interaction parameters for the symmetric Berman model of mixing are given in Table 8 (from where the G°_{298} and H°_{298} values were taken).

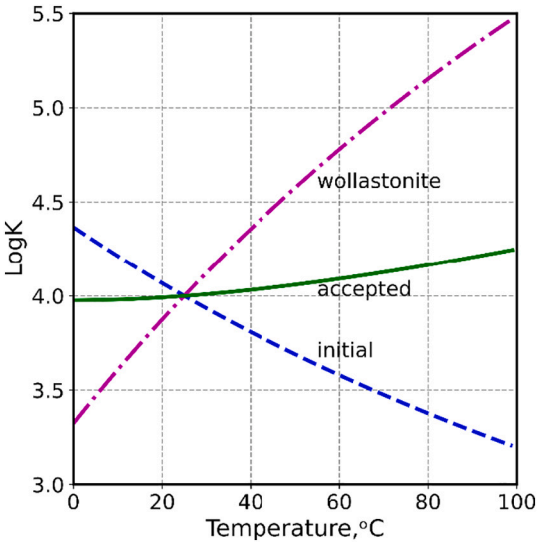

Fig. 9. Temperature variation of logK of reaction $Ca^{2+} + SiO_3^{2-} = CaSiO_3^0$ (at 1 bar) for three cases described in the text and in Table 9.

phase) model [2]. The minimal DSP model consists of three phases [70–72], which is clearly not enough to mimic the behaviour of the CASH+ model (e.g. Walker et al. [2] discretized their two C-S-H non-ideal solid solutions into a DSP model with 12 "phases") [2]. The discretization procedure consists in splitting the variable composition of the phase in equilibrium into a finite number of *pseudocompounds* or "frozen" bulk compositions x, each treated then as a pure phase with its $V^{\circ}_{x,\,298}$, $G^{\circ}_{x,\,298}$ or $\log K^{\circ}_{x,\,298}$ values and temperature corrections (e.g. via the $H^{\circ}_{x,\,298}$ value). In this way, a continuous equilibrium solid solution model is converted into a discrete set of solid stoichiometries over a selected compositional space. One or two of those "frozen" phases will then be stable at any given conditions and composition of the system of interest. The number and stepping of discrete x phases define how good the solid solution solubility is approximated by a DSP model.

This is also the case of the CASH+ sublattice solid solution model, which runs natively (with internal smoothing) in GEMS codes, but which is hard to implement in PHREEQC and similar chemical speciation solvers. In order to make it possible for PHREEQC users of the Cemdata18 database to work with the CASH+ core model, we have discretized it in a semi-automatic mode using the GEM-Selektor and ThermoMatch codes, as described in detail in Appendix B1 (Supporting Material), including the generated reactions with log$K$ values exported into PHREEQC.dat format, to be also added to the next edition of Cemdata database (https://www.empa.ch/cemdata). Test calculations show that this DSP CASH+ model reproduces the C-S-H solubility with increasing C/S ratio in a stepwise appearance (Fig. 12) both in PHREEQC and in GEMS codes. The horizontal "steps" correspond to co-existence of two pseudo-compound phases or one of them together with $SiO_{2(am)}$ or portlandite.

4. Discussion

4.1. Previous solid solution models of C-S-H

Thermodynamic solid solution models of C-S-H are in use since 1990s (see recent overviews in [2,4]). They can predict the solubility, density, water content of C-S-H, but most of them are not structurally consistent and are not incremental. The reason of that is that end-member stoichiometries were often chosen arbitrary (e.g. SiO_2(am) and $Ca(OH)_2$(cr) or tobermorite and $Ca(OH)_2$(am) [2,73]), and they are not compatible with the defect-tobermorite or jennite structures, thus forcing an introduction of the "artificial" non-ideal mixing. Some old models were developed in the right direction, starting from the structural reasoning, but then had to undergo radical simplifications, such as a "downscaling" of endmember stoichiometries [3,4] in order to comply with the thermodynamics of a simple ideal mixing model, available in most speciation codes as the default or the only option.

Two- or one-phase simple ideal solid solution models [3,74,75] were derived from an assumption that there is a mixing between a tobermorite-like endmember with C/S = 5/6 and a jennite-like endmember with C/S = 10/6 (forming a CSH-II solution phase), sometimes supported by another assumption of mixing between $SiO_{2(am)}$ and the tobermorite-like C/S = 5/6 endmember (CSH-I phase) to be able to obtain C-S-H compositions with C/S < 5/6. Note that the CSH-I phase was excluded from the Cemdata database [5]. These simple models produced quite reasonable curves for C-S-H solubility, but could not be extended incrementally to cover the uptake of K, Na and other cations (such as Zn, [76], or U^{VI} [77]). In other words, adding a new cation required to re-adjust the standard Gibbs energy values and stoichiometries of all endmembers, including those without this cation. Besides, recent structural studies of C-S-H converged on assuming the defect-tobermorite structure of C-S-H in the whole range of compositions, no more supporting the involvement of jennite structure ([15] and refs. therein).

In the next-stage study aimed to address some of these issues [4], the defect-tobermorite structure was the only assumption, in which four kinds of structural sites with possible substitutions were identified: BT (bridging tetrahedral in silicate chain), IC (interlayer cation), CU (extra calcium unit in interlayer) and IW (interlayer water). The model was simplified by lumping BT and IC sites together into the BTI site, and fixing the composition of IW sites. Out of this, two alternative ideal solid solution models were constructed (both capable of reproducing the solubility and the MCL as function of C/S ratio): quaternary CSHQ and ternary CSH3T models [4].

The CSHQ solid solution model, included in Cemdata18 thermodynamic database [27], consists of four downscaled endmembers. With zero enthalpy of mixing, it fits most published C-S-H solubility data sets (by adjusting end-member $G^{\circ}_{j,298}$ within 1 to 3 kJ·mol^{-1}), also includes temperature trend up to 80–100 °C, and reproduces the MCL and volume trends of C-S-H vs C/S ratios in the presence of liquid water. Note that CSHQ (along with CSH3T) model reproduces the water content in C-S-H including the "gel pore water". The theoretical range of C/S ratio is 0.67 to 2.25, though in equilibrium limited by the presence of SiO_2(am) to C/

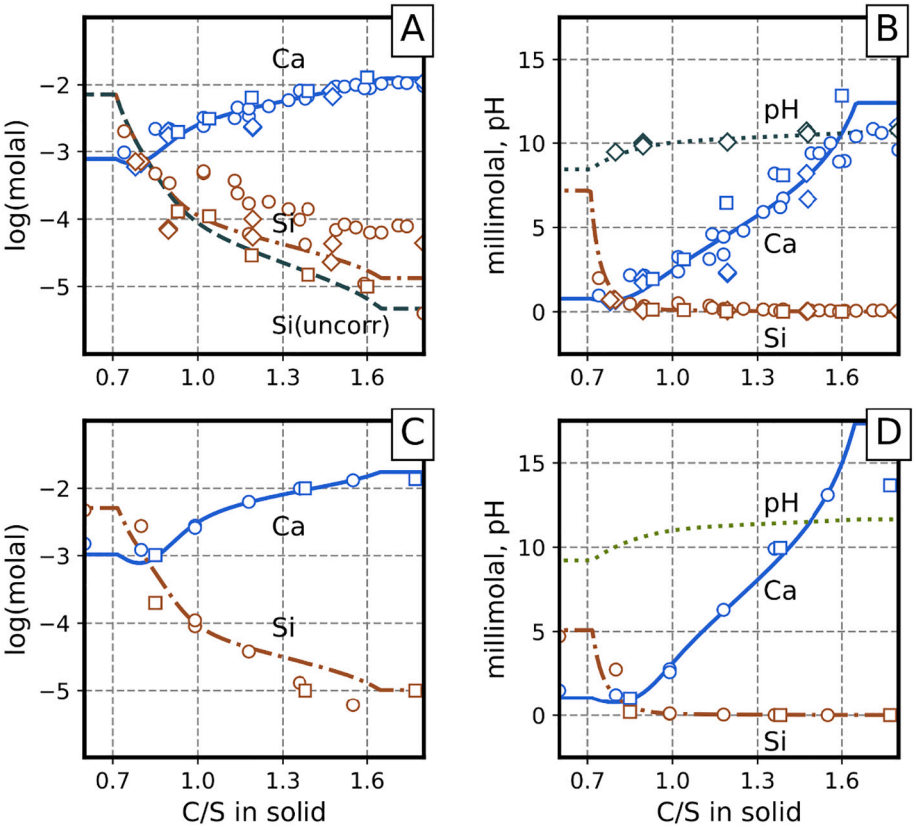

Fig. 10. Profiles of $[Ca]_{aq}$, $[Si]_{aq}$ and pH predicted by the CASH+ core model for temperatures 90 °C (A,B) and 50 °C (C,D). Experimental data in (A, B): [64], 90 °C, circles; [65], 85 °C, diamonds; Ph.D. Thesis by R. Barbarulo (2002, Comportment de materiaux cimentaries: actions des sulfates et de la temperature. PhD thesis, L'Universite Laval, Quebec, Canada), 90 °C, squares. Data in (C, D): [66], 55 °C, circles; [67], 50 °C, squares.

S > 0.7 and by $Ca(OH)_2$(cr) to C/S < 1.64). In the presence of alkali metals, the composition of C-S-H in equilibrium with portlandite has C/S < 1.5, depending on the alkali concentration in porewater [54]. In this range, C-S-H can be modelled using a somewhat simpler ideal CSH3T solid solution model with three endmembers and zero excess enthalpy [4], more consistent with defect-tobermorite structure and spectroscopic data on low-Ca (nanocrystalline) C-S-H, including the account for ordering around C/S = 1.0.

The CSH3T model was derived assuming that CU sites only contain vacancy (i.e. there are no additional "calcium hydroxide units" in the interlayer), but the BTI sublattice is split into two sublattices – BTI1 and BTI2, – in both the silica species can be substituted by calcium one. This is a solid solution model of (A,B)(A,B)X type, similar to that used for dolomite, in which the extent of ordering is defined by an internal reaction 0.5TobH + 0.5T2C = T5C between the endmembers, with the Gibbs energy effect

$$\Delta_r G^{\mathrm{ord}}_{298} = G^{\circ}_{298}(\mathrm{T5C}) - 0.5G^{\circ}_{298}(\mathrm{TobH}) - 0.5G^{\circ}_{298}(\mathrm{T2C})$$

In this model, the extent of ordering can be adjusted by tweaking the $G^{\circ}_{j,\,298}$ value of the intermediate "pentameric" T5C endmember with C/S = 1.0. The CSH3T model fits the experimental C-S-H solubility data (from co-precipitation or double-decomposition experiments) more precisely than CSHQ, but limited to C/S = 1.5 in C-S-H. It also reproduces well the MCL (structural) data.

There were later attempts to extend the CSH3T model for the uptake of other cations: Na^+ and Al^{3+} (CNASH model, [6]) and UO_2^{2+} [77]. Although capable of describing the cation uptake isotherms satisfactorily, all extensions based upon the CSH3T downscaled model have the same shortcoming: the lack of incrementality. This means that adding a cation endmember(s) required the re-adjustment of G°_{298} of all endmembers, including those without the added cation. Besides, the downscaling of crystallographic formulae of endmembers resulted in atomistically infeasible fractional stoichiometries of ionic moieties. The Vanselow rule for interlayer cation exchange (Na + for Ca^{2+} instead of Na^+ for $Ca_{0.5}{}^+$) was also not satisfied. A rigorous extension of the CSH3T model to clinker hydration products with C/S > 1.5 was not possible. The need in the 'ordered' T5C endmember may result from neglecting strong non-ideal interactions in BT and IC sites, such as found in the CASH+ core model (see Table 9).

These drawbacks of existing C-S-H solid solution models, along with the need for extensions with minor components, especially Al, Fe^{III} and alkali cations, and for better structural plausibility, motivated us for developing the new sublattice CASH+ model, described in this contribution and in companion papers about its incremental extensions.

4.2. Solid solution vs surface complexation models of C-S-H

A common criticism of C-S-H solid solution models consists in that they do not account explicitly for the surface complexation and ion exchange on outer surfaces of C-S-H particles [78], where important phenomena occur such as an "overcharging" of surfaces by the sorption of Ca^{2+} ions [79]. The typical approach to develop a surface complexation model for C-S-H consists in defining the amount of surface sites per unit mass of C-S-H (usually expressed in dry oxides SiO_2 and CaO) and then defining surface complexes on edges (Ca-OH and silanol Si-OH surface groups) and on the outer basal planes [55] via the respective surface complexation reactions and (optionally) the electrostatic model corrections when the surface charge becomes positive or negative. Such surface complexation models can be parameterized against the experimental sorption isotherms (of cation adsorption) at a given pH or against the so-called pH sorption edges (at a given cation loading in the system). Advanced electrostatic models that involve electrolyte adsorption and

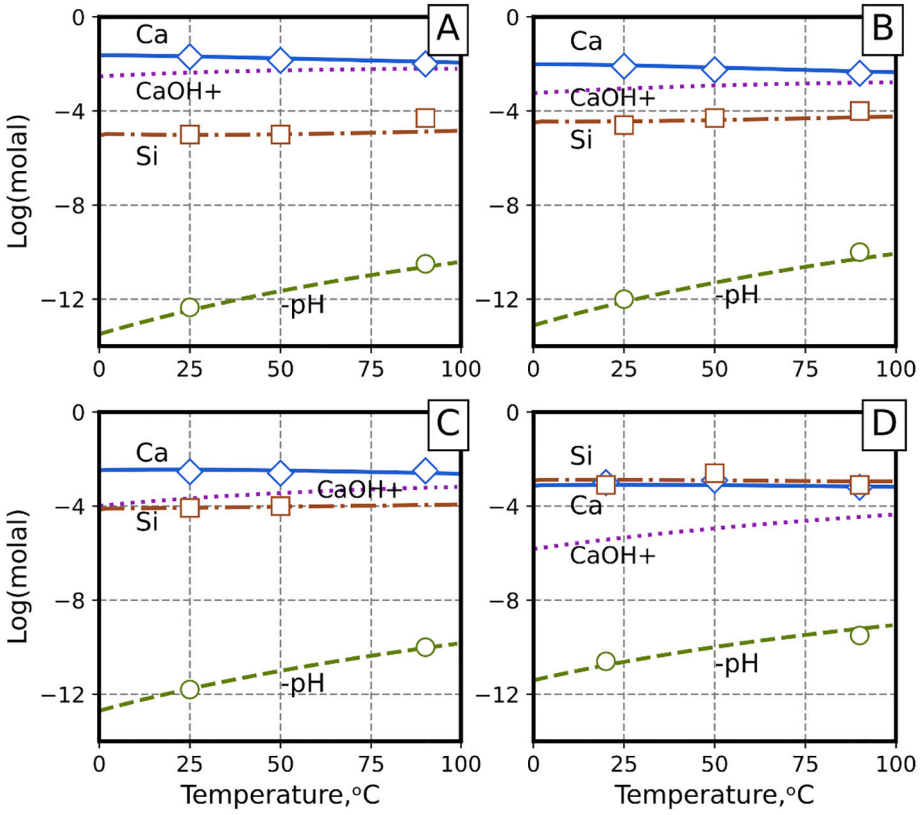

Fig. 11. Blind-predicted temperature trends of total aqueous dissolved Ca, Si and -pH: C-S-H with C/S > 1.6 in equilibrium with CH (A); with C/S = 1.2 (B); with C/S = 1.0 (C) and with C/S = 0.8 (D). Scattered symbols show typical experimental values at 20–25 °C, 50 °C and 90 °C (from the same data sets as in Fig. 10). Molality of $CaOH^+$ complex (included into $[Ca]_{aq}$) is shown as a dotted curve.

Table 11
Standard molar thermodynamic properties for C-S-H structural formulas as reported in Roosz et al. [57] at T = 25 °C (298.15 K), P = 1 bar (0.1 MPa) compared with values from the CASH+ model.

Phase	Structural formula	G°_{298}, J·mol^{-1}		S°_{298}, J·(mol·K)$^{-1}$		Cp°_{298}, J·(mol·K)$^{-1}$		V°_{298}, cm^3·mol^{-1}	
CSH06	Ca0.69SiO2.415(OH)0.55:0.68H2O	**−1554.89**	*−1555.79*	**117.50**	*131.23*	**111.98**	*121.50*	**45.5**	*52.4*
CSH10	Ca1.06SiO2.725(OH)0.67:0.89H2O	**−1870.99**	*−1871.23*	**122.00**	*137.70*	**123.54**	*129.87*	**53.0**	*60.4*
CSH12	Ca1.23SiO2.865(OH)0.73:1.06H2O	**−2031.21**	*−2032.40*	**139.20**	*161.81*	**139.61**	*150.37*	**56.9**	*61.8*
CSH16	Ca1.41SiO2.96(OH)0.90:1.12H2O	**−2185.73**	*−2185.74*	**153.00**	*180.28*	**152.67**	*178.12*	**61.5**	*68.2*

Boldface: values from the CASH+ core model; italic: values from Roosz et al. [57].

based on the Stern layer concept are capable of predicting the surface charge density and modelling the electrophoretic data (zeta-potentials).

However, surface complexation models, mostly developed for experimental systems with low solid/water ratios, typically require a priori knowledge of composition (C/S ratio) and mass of C-S-H relative to aqueous solution (s/w mass ratio). In thermodynamic systems describing cements, it is often impossible to know both parameters before modelling of equilibrium with dozens of other hydrated cement phases. This equilibrium also defines pH, pe (redox potential), and composition of the porewater. Therefore, setting the amounts of sorption sites for C-S-H becomes a non-thermodynamic procedure, solely dependent on the user's expertise.

Surface complexation models are good for describing strong adsorption of minor and trace cations such as base metals, REE or actinides, onto very stable or non-reactive hydroxylated surfaces such as on rutile TiO_2, magnetite Fe_3O_4, hematite Fe_2O_3, goethite FeOOH, alumina Al_2O_3, or quartz SiO_2. All these minerals, in form of nano- or submicron-size particles, are hardly soluble or insoluble in water, and have large specific surface areas. In such systems, the amounts of surface sites can be fixed well, and this stabilizes other components of the surface complexation model. In this context, C-S-H phases are bad candidates because of their high reactivity and fast re-precipitation with different composition in the absence of buffering phases ($SiO_{2(am)}$ or portlandite). The specific surface area of C-S-H, although usually high (up to 250 m^2·g^{-1}), is not at all stable or persistent, and may change significantly with C/S ratio, time or temperature. For all those reasons, surface complexation models will always face difficulties to reliably describe the stability and solubility of C-S-H as function of its composition.

Keeping up with the solid solution models of C-S-H, one has to know how much those can be biased by neglecting the impact of the surface complexation occurring on edge- and basal surfaces of C-S-H particles exposed to “gel” pores (the ions in the interlayers are included into the solid solution model). This question has not yet been investigated in detail, but some qualitative arguments are possible. The typical C-S-H geometry varies greatly from the needle-like shapes to the deformed platelets [33,80,81] made of a few stacked tobermorite-like layers. In such platelets, the area of outer basal surfaces is about 1/5 to 1/6 of the total basal area. Assuming that the binding BT sites on outer basal surfaces are similar to those in the interlayer and that the exchange ion populations in both locations are not very different (probably outer basal surfaces can be enriched in Ca^{2+} ions compared to interlayer

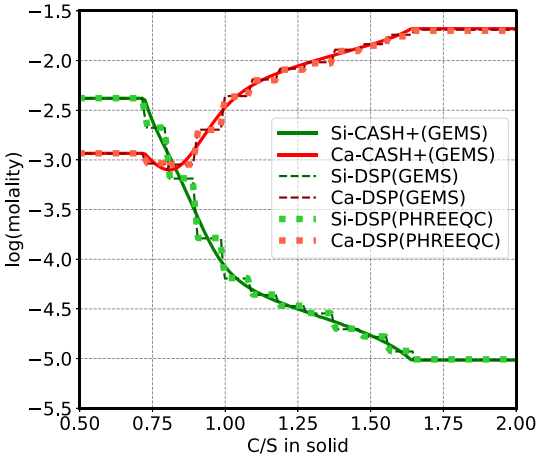

Fig. 12. Comparison between the calculated C-S-H solubility using the CASH+ model in GEM-Selektor (continuous lines) and the DSP model in PHREEQC (dashed lines) and GEM-Selektor (symbols) (11 discrete pseudocompounds, CSH072 to CSH165, see reactions in Appendix B1, Supporting Material).

surfaces), we can estimate the bias as several percent of the Ca content. This can be accommodated during parameterization of the solid solution model. The effect of broken bonds on C-S-H particle edges is more difficult to evaluate, but, keeping in mind that, similar to clays [82], the specific surface area of edge surfaces should not exceed 8–10 $m^2 \cdot g^{-1}$ (total SSA > 150 $m^2 \cdot g^{-1}$), the bias in estimating the cation sorption due to edge sites should be about 6% or less. This also can be accommodated (based on experimental solubility and sorption data) in the parameterization of the solid solution model. It is also known that cross-linking of silica chains in the C-S-H interlayer and decreasing interlayer spacing do not influence strongly the stability/solubility of C-S-H [6].

4.3. Impact of aqueous speciation

Aqueous Ca speciation is dominated by Ca^{2+} ion in the whole C/S interval, totally at C/S < 0.8, whereas the $Ca(OH)^+$ hydroxocomplex comprises 5% at C/S = 1.0 to 13% at C/S = 1.64 in presence of portlandite (Fig. 5, C).

As seen in Fig. 5, C, the $CaSiO_3^0$ aqueous complex (written as $CaH_2SiO_4^0$ in [83], [61]) comprises <1% of total dissolved $[Ca]_{aq}$, but dominates the aqueous Si speciation at C/S > 1.1 in C-S-H. At bulk C/S > 1.6, this complex binds >90% of the total dissolved $[Si]_{aq}$ [2]. Therefore, the adjustment of G°_{298} value of this species must have a strong influence on the CASH+ model behaviour and on the optimized G°_{298} values of some of its endmembers.

Several values were reported for the stability of $CaSiO_3^0$ ($CaH_2SiO_4^0$) at 1 bar and 25 °C, differing in more than 1.5 pK units (ca. 6 kJ·mol^{-1}). The G°_{298} = 1517.56 kJ·mol^{-1} value from the PSI-Nagra database 12/07 [28] was derived from a single set of results of potentiometric titrations of $Si(OH)_4^0$ in the presence of Ca^{2+} and Mg^{2+} in 1 M $NaClO_4$ up to pH = 9 reported in [83]. Walker et al. [2] used the solubility data on C-S-H to better constrain the stability of this species, and obtained a value 0.6 pK units less stable than the one from [83]. Their reported value of log$K$ = 4.0 (for the reaction $Ca^{2+} + H_2SiO_4^{2-} = CaH_2SiO_4^0$) and our results (Table 8) converge to the G°_{298} value of $CaSiO_3^0$ equal to −1514.14 kJ·mol^{-1}. Nicoleau and Schreiner [61] determined the stability of calcium silicate species at 25 °C using an ion selective electrode method. From the reported formation constant of log$K$ = 2.9 in [61] and the data for SiO_3^{2-} and Ca^{2+} from the PSI-Nagra database, a value of −1507.85 kJ·mol^{-1} was calculated for G°_{298} of this species (actually taken as the initial value for GEMSFITS parameterization). Other thermodynamic properties of $CaSiO_3^0$ complex have been discussed above, in the section about the temperature trends of the CASH+ solid solution model.

Another Ca-Si aqueous complex in consideration was $CaHSiO_3^+$ ($CaH_3SiO_4^+$), whose stability was also first estimated by [83]. This complex was not included into our optimizations because of its minor contributions to both $[Si]_{aq}$ and $[Ca]_{aq}$ in the whole interval of C/S ratios (Fig. 5, C). The $HSiO_3^-$ species dominates $[Si]_{aq}$ at 0.8 < C/S < 1.1, and takes about 50/50 share with SiO_2^0 ($Si(OH)_4^0$) silica species at C/S < 0.7 in the presence of $SiO_{2(am)}$ phase.

Given the importance of aqueous Ca-silica complexes for the C-S-H solubility, it would be interesting to independently check their stability by molecular dynamics (MD) simulations. Nicoleau and Schreiner [61] first performed a DFT study using the COSMO-RS solvation model and the related software. Their modelling results corroborated the two most stable complexes $CaH_2SiO_4^0$ (prevails under highly alkaline conditions) and $CaH_3SiO_4^+$ (prevails at moderately alkaline conditions). However, in that DFT modelling exercise, only properties of two reactions combining these complexes with a hypothetical neutral $Ca(H_3SiO_4)_2^0$ complex were determined (see Table 2 in [61]). The latter species is deemed to be relatively unstable and totally insignificant in Si speciation in the experimental range [61], and its formation equilibrium constant is unknown. Hence, so far, the DFT results (having the estimated 2.0 kcal·mol^{-1} or 1.5 pK uncertainty) have provided little to constrain the stability of $CaH_2SiO_4^0$ ($CaSiO_3^0$) complex better than this could be done on the basis of fitting the CASH+ solid solution models to C-S-H solubility datasets.

4.4. Impact of the type of non-ideal interactions

As described in more detail in Appendix A1, we tested parameterization of the CASH+ core model for Ca-Si-H_2O subsystem using alternatively three styles of excess Gibbs energy interaction parameters for substitutions of moieties in BT and IC sublattices: Berman symmetric, Berman pseudo-ternary (with- or without symmetric), and CEF symmetric. We have found that more complex styles with more interaction parameters do not significantly improve the overall quality of fits and the least-square sums of residuals. Therefore, the simplest (Berman symmetric) approach with 4 interaction parameters is recommended (as given in Table 8).

Examining the resulting values of interaction parameters (Table A1-4 in Supplementary Material; Table 8) shows that the only parameter $^{IC}W_{Cv}$ – the energy of interaction between Ca and vacancy in IC sites – has large negative and very similar values in both fit variants (−17.1 ± 1.8 vs −17.3 ± 1.6 kJ·mol^{-1}), which points at a rather strong tendency to maintain about equal site fractions of both moieties. This tendency is clearly seen in Fig. 5, D at C/S > 0.8; at lower C/S ratios, this site is dominated by vacancies due to the lack of Ca^{2+} ions, as expected. The interaction between silica and vacancy moieties in BT sites, $^{BT}W_{Sv}$, also shows large negative energies in both Step 5 and Step 4 variants (−19.1 ± 0.5 and −16.1 ± 1.0 kJ·mol^{-1}, respectively). Indeed, similar site fractions of both moieties are observed at 1.0 < C/S < 1.5, also showing that Ca moiety occupies large fraction of BT sites much later than Ca occupies IC sites (Fig. 5 C,D), in accordance with the atomistic considerations presented in [15].

The other two interaction parameters in BT sites, namely $^{BT}W_{CS}$ between Ca and Si moieties and $^{BT}W_{Cv}$ between Ca and vacancies, show different values in fitting Step 4 and Step 5. In Step 4 (that results in C/S = 1.5 at the appearance of portlandite, see Fig. 4 and Table A1-4 in Supplementary Material), both interaction parameters are strongly to moderately negative (−17.7 ± 5.4 and −12.0 kJ·mol^{-1} ± 6.2 kJ·mol^{-1}, respectively), though they show quite large Monte-Carlo confidence intervals in comparison with the previous two interaction parameters. In Step 4 fits, this means a tendency of all three moieties to be present in about equal site fractions. However, in Step 5 fits (where portlandite appears at C/S = 1.64, i.e. C-S-H compositions around C/S = 1.6 are more stable than in Step 4 fits), the interaction parameters $^{BT}W_{CS}$ and $^{BT}W_{Cv}$ are much less negative (−8.6 ± 1.8 and − 7.9 kJ·mol^{-1} ± 0.7 kJ·mol^{-1}, respectively, Table 8), letting the Ca moiety to stronger

dominate at low Si moiety site fractions, thus making C-S-H more stable at high C/S ratios.

A peculiar feature of sublattice solid solution models with the reciprocity of endmembers is that different combinations of them can alternatively describe the same bulk composition and other bulk properties of the solid solution (density, molar Gibbs energy, heat content, mean chain length). As long as different variants of the model at given bulk elemental composition of the phase produce the same site fractions of moieties and the same bulk properties, they are considered equivalent, even if mole fractions of endmembers are different. For instance, the CASH+ core model consists of six endmembers, but only four of them are sufficient to describe any given bulk elemental composition. Because of this, the numerical solution for the equilibrium speciation may depend on the choice of the initial guess. In Appendix A1.4 (Supporting Material), possible initial guesses were tested using the GEM-Selektor code, and reasonable combinations were recommended as variants 5, 5a, 5b. Across the compositional space (C/S ratio), these variants result in identical profiles of site fractions of moieties, mole fractions of endmembers, density, volume and other properties, easily interpretable in terms of changing the defect-tobermorite structure upon loading with Ca^{2+} ions.

4.5. CASH+ core model parameter uncertainties

The 95% (two-sigma) confidence intervals for the fitted parameters, retrieved using the Monte Carlo method as implemented in GEMSFITS code [29], are given in Table A1-4 in Supplementary Material and in Table 8. Regarding the standard Gibbs energies of CASH+ model endmembers, there are two groups. TSCh, TSvh and Tvvh (polymeric and dimeric with vacant interlayer) endmembers have 95% confidence intervals $\delta^{\circ}G_{298} < 1.1$ kJ·mol^{-1} (<0.2 pK units), whereas the δG°_{298} values for TCCh, TCvh and TvCh endmembers (dimeric) are within 1.27 and 4.96 kJ·mol^{-1} (0.22 to 0.87 pK). All these uncertainty intervals appear to reflect the scatter and error of experimental solubility data in the datasets selected for parameterization runs. The estimated confidence intervals δW of Berman symmetric interaction parameters are all below 2 kJ·mol^{-1} in the recommended model parameterization (Table 8) along with the δG°_{298} of $CaSiO_3^0$ aquo-complex, whereas in the Step 4 fit (Table A1-4 in Supporting Material), two parameters ${}^{BT}W_{CS}$ and ${}^{BT}W_{Cv}$ have got δW values above 5.3 kJ·mol^{-1} (and much more negative values of these parameters than fitted in Step 5 (Table 8)). The reason of this difference is not quite clear, although it seems that an additional constraint imposed in Step 5 that the C/S = 1.65 in C-S-H in presence of portlandite had a beneficial effect on uncertainties of all model parameters, especially of the latter two interaction parameters. The Monte-Carlo estimated confidence intervals appear realistic also because they have comparable absolute values with the parameter differences between Step 4 and Step 5 fits (Table 8; Table A1-4 in Supplementary Material).

5. Concluding remarks

In this contribution, using the sublattice solid solution approach, we present a newly developed, flexible and extendable CASH+ model describing stability, solubility, density, water content and MCL of C-S-H phases, in consistency with the modern atomistic view of the C-S-H defect-tobermorite structure [14,15]. The CASH+ model is based on considering the simultaneous substitutions of chemical moieties in BT (bridging tetrahedral in silicate chain) and IC (interlayer cation exchange) sublattices (Table 1), while the IW (interlayer water) sites for now contain H_2O molecules that can be replaced by vacancies in future development of the CASH+ model for low relative humidity or higher temperatures. It is assumed that no substitutions occur in silicate - calcium layer dimeric units (DU). The stoichiometries of chemical moieties on IC and BT sites were chosen such that the solid water content in C-S-H would be correctly reproduced in the whole range of molar C/S ratios. Based on this scheme, all possible solid solution endmembers can be generated by permutation (Table 2). The model was fine-tuned by the GEMSFITS parameterization, based on a careful selection of the experimental solubility and spectroscopy data.

To start the fitting of CASH+ model parameters, reasonable initial estimates of standard molar thermodynamic properties of endmembers were needed, keeping in mind that most such endmembers do not exist as pure minerals. The estimates of standard entropy, heat capacity and molar volume at $P = 1$ bar and $T = 25$ °C are also needed for a correct representation of temperature trends of the CASH+ stability and solubility, as well as the solid density. To build a consistent dataset of such estimates, we combined the isocoulombic reactions with the VBT (volume-based thermodynamics) [31] and the polyhedral contributions [40] methods, to estimate standard properties of CASH+ endmembers in the system Ca-Si-K-Na-Al-Si-H_2O with the uncertainty of 1% for G^*_{298} and H^*_{298}, 10% for S^*_{298} and 30% for Cp^*_{298} estimates. Because of the lack of experimental data at elevated temperatures, the standard values of entropy, heat capacity and molar volume were not further optimized, but used as is, wherever appropriate, also in further extensions of the model [24–26].

The sublattice solid solution model of mixing with reciprocal terms, as used in the CASH+ model, allows three different styles of excess energy interaction parameters (see details in Appendix A1, Supplementary Material): Berman symmetric (binary), Berman pseudo-ternary (optionally with symmetric interaction parameters), and CEF (Compound Energy Formalism) with binary interaction parameters. In GEM-Selektor and GEMSFITS implementation, these styles can be used alternatively. Of these, the Berman symmetric style is the simplest and needs the minimum number of binary interaction parameters between different moieties substituting in the same sublattice (e.g. four parameters for the CASH+ core model in Ca-Si-H_2O system). The parameterization trials in the CASH+ core system showed that more complex styles do not provide any significant improvement of fits or minimal objective function values relative to the simplest Berman symmetric style, which is therefore recommended for further use.

The strategy of parameterization of the CASH+ core model for Ca-Si-H_2O sub-system (6 endmembers, 4 interaction parameters) involved a large selection of experimental data on C-S-H solubility at ambient conditions, along with the structural information such as MCL derived from the ^{29}Si MAS NMR spectroscopy data. After performing all five steps of the parameterization strategy, the internally consistent data set was obtained (i.e. standard properties of endmembers plus values of four interaction parameters, Tables 8, 10), shown to describe well the experimental data, including the solid density, water content, and MCL at ambient temperature. Tests at different C/S ratios showed rather flat temperature curves (in the interval 0 to 100 °C), except pH that significantly decreases with increasing temperature; the CASH+ model reproduces temperature trends without any additional fitting of standard properties of endmembers and interaction parameters.

The core CASH+ model, with its parameters optimized and fixed, lays down the foundation for incremental and consistent extensions with endmembers containing alkali and alkali-earth cations [24], aluminum and Fe^{3+} [25], and other cations (Zn, actinides, REE) of interest for waste management and disposal [26].

After parameterization, the CASH+ model with extensions will be provided in the next edition of the Cemdata database to be directly used in GEM-Selektor for an improved modelling of equilibrium solid- and pore-water composition in hydrated cement materials. A discretized (DSP) variant of CASH+ model has been generated for use in PHREEQC and similar LMA codes that are not capable of solving the equilibrium speciation involving sublattice solid solutions (Appendix C1, Supplementary Material).

6. Key points of this study

1. The new sublattice solid solution CASH+ core model (Ca-Si-H_2O subsystem, Table 8, 10) is capable to accurately describe the experimental data for synthetic (double-decomposition or co-precipitation) C-S-H solubility, along with the available structural MCL data (derived from ^{29}Si NMR spectroscopy), density, and non-gel water content (molar H_2O/Si ratios, derived from ^{1}H NMR, neutron scattering, and isotherms data).
2. Large negative (−10 to −20 kJ·mol^{-1}) Berman symmetric non-ideal interaction parameters are needed in the reciprocal sublattice solid solution model to describe the measured chemical aqueous solid composition along with together with the mean silicate chain length structural data.
3. The CASH+ core model, without any additional fitting, is shown to be applicable from 10 to 90 °C for modelling the solubility, MCL and density data.
4. $CaSiO_3^0$ is the dominant silica species at C/S > 1.15 mol ratio in C-S-H; having this complex too weak results either in an over-prediction of $[Si]_{aq}$ at C/S > 1.2 and especially in equilibrium with portlandite, or in some strongly over-fitted parameters of the CASH+ model. For a better agreement with the measured data, the G°_{298} value of $CaSiO_3^0$ was fitted together with other CASH+ model parameters to a value −1514.14 kJ·mol^{-1} (corresponding to logK_{298} = 4.0 for the reaction $Ca^{2+} + SiO_3^{2-} = CaSiO_3^0$).
5. With stepwise incremental extensions (described in companion papers [24–26]), the model can be further applied potentially to the uptake other cations and anions in C-S-H, as well as extended to partially dehydrated states. One of the challenges is how to separate the cations bulk incorporation from surface adsorption in C-S-H.
6. A combination of structural/atomistic studies of C-S-H with modern flexible and incrementally expandable thermodynamic solid solution models, GEMS and GEMSFITS codes, opens up new perspectives in chemical thermodynamic studies of cement systems as construction materials and as waste matrices/barriers.

CRediT authorship contribution statement

Dmitrii A. Kulik: Conceptualization; Methodology; Software; Investigation; Formal analysis; Visualization; Validation; Writing - original draft; Writing - review & editing.

George Dan Miron: Investigation; Formal analysis; Software; Visualization; Validation; Writing - original draft; Writing - review & editing.

Barbara Lothenbach: Supervision; Investigation; Validation; Writing – review & editing; Resources; Project administration.

Declaration of competing interest

The authors declare that they have no known competing financial interests or personal relationships that could have appeared to influence the work reported in this paper.

Acknowledgments

The funding from SNF CASH-2 project 200021_169014/1 and the SNF Sinergia CASH project 130419, as well as partial financial support from Nagra, Wettingen, are gratefully acknowledged. The study benefited greatly from insightful discussions with Paul Bowen, Karen Scrivener, Sandra Galmarini, Aslam Kunhi Mohamed, Sergey Churakov, Urs Berner, Michael Kersten, Andre Nonat, Erich Wieland, Jan Tits and many other colleagues.

Appendix A. Supplementary Material

Appendices A1, B1, C1 provide technical details on solid solution thermodynamics, GEMS implementation, parameter optimizations, model discretization for PHREEQC, and other information for expert readers. The Supplementary Material to this article can be found online at doi: https://doi.org/10.1016/j.cemconres.2021.106585.

References

[1] B. Lothenbach, A. Nonat, Calcium silicate hydrates: solid and liquid phase composition, Cem. Concr. Res. 78 (2015) 57–70.
[2] C.S. Walker, S. Sutou, C. Oda, M. Mihara, A. Honda, Calcium silicate hydrate (C-S-H) gel solubility data and a discrete solid phase model at 25 °C based on two binary non-ideal solid solutions, Cem. Concr. Res. 79 (2016) 1–30.
[3] D.A. Kulik, M. Kersten, Aqueous solubility diagrams for cementitious waste stabilization systems: 2. End-member stoichiometries of ideal calcium silicate hydrate solid solutions, J. Am. Ceram. Soc. 84 (2001) 3017–3026.
[4] D.A. Kulik, Improving the structural consistency of C-S-H solid solution thermodynamic models, Cem. Concr. Res. 41 (2011) 477–495.
[5] T. Matschei, B. Lothenbach, F.P. Glasser, Thermodynamic properties of Portland cement hydrates in the system $CaO-Al_2O_3-SiO_2-CaSO_4-CaCO_3-H_2O$, Cem. Concr. Res. 37 (2007) 1379–1410.
[6] R.J. Myers, S.A. Bernal, J.L. Provis, A thermodynamic model for C-(N-)A-S-H gel: CNASH_ss. Derivation and validation, Cem. Concr. Res. 66 (2014) 27–47.
[7] D. Kulik, G.D. Miron, B. Lothenbach, A realistic three-site solid solution model of C-S-H, in: Goldschmidt Abtracts 2018, 2018, p. 1364.
[8] G. Renaudin, J. Russias, F. Leroux, C. Cau-dit-Coumes, F. Frizon, Structural characterization of C–S–H and C–A–S–H samples—part II: local environment investigated by spectroscopic analyses, J. Solid State Chem. 182 (2009) 3320–3329.
[9] G. Renaudin, J. Russias, F. Leroux, F. Frizon, C. Cau-dit-Coumes, Structural characterization of C–S–H and C–A–S–H samples—part I: long-range order investigated by Rietveld analyses, J. Solid State Chem. 182 (2009) 3312–3319.
[10] S. Grangeon, F. Claret, C. Lerouge, F. Warmont, T. Sato, S. Anraku, C. Numako, P. Linard, B. Lanson, On the nature of structural disorder in calcium silicate hydrates with a calcium/silicon ratio similar to tobermorite, Cem. Concr. Res. 52 (2013) 31–37.
[11] S. Grangeon, F. Claret, C. Roosz, T. Sato, S. Gaboreau, Y. Linard, Structure of nanocrystalline calcium silicate hydrates: insights from X-ray diffraction, synchrotron X-ray absorption and nuclear magnetic resonance, J. Appl. Crystallogr. 49 (2016) 771–783.
[12] I.G. Richardson, The calcium silicate hydrates, Cem. Concr. Res. 38 (2008) 137–158.
[13] J. Li, G. Geng, R. Myers, Y.-S. Yu, D. Shapiro, C. Carraro, R. Maboudian, P.J. M. Monteiro, The chemistry and structure of calcium (alumino) silicate hydrate: a study by XANES, ptychographic imaging, and wide- and small-angle scattering, Cem. Concr. Res. 115 (2019) 367–378.
[14] A. Kunhi Mohamed, P. Moutzouri, P. Berruyer, B.J. Walder, J. Siramanont, M. Harris, M. Negroni, S.C. Galmarini, S.C. Parker, K.L. Scrivener, L. Emsley, P. Bowen, The atomic-level structure of cementitious calcium aluminate silicate hydrate, J. Am. Chem. Soc. 142 (2020) 11060–11071.
[15] A. Kunhi Mohamed, S.C. Parker, P. Bowen, S. Galmarini, An atomistic building block description of C-S-H - towards a realistic C-S-H model, Cem. Concr. Res. 107 (2018) 221–235.
[16] M. Hillert, Phase Equilibria, Phase Diagrams and Phase Transformations: Their Thermodynamic Basis, Cambridge University Press, Cambridge, 1998.
[17] H.L. Lukas, S. Fries, B. Sundman, Computational Thermodynamics: The Calphad Method, Cambridge University Press, Cambridge, 2007.
[18] G.D. Miron, D.A. Kulik, B. Lothenbach, Parameterization of a new C-S-H solid solution model for alkali uptake, Goldschmidt Abstracts, 2018 (2018) 1778.
[19] M.R. Andalibi, A. Kumar, B. Srinivasan, P. Bowen, K. Scrivener, C. Ludwig, A. Testino, On the mesoscale mechanism of synthetic calcium–silicate–hydrate precipitation: a population balance modeling approach, J. Mater. Chem. A 6 (2018) 363–373.
[20] S.V. Churakov, C. Labbez, Thermodynamics and molecular mechanism of Al incorporation in calcium silicate hydrates, J. Phys. Chem. C 121 (2017) 4412–4419.
[21] S.V. Churakov, C. Labbez, L. Pegado, M. Sulpizi, Intrinsic acidity of surface sites in calcium silicate hydrates and its implication to their electrokinetic properties, J. Phys. Chem. C 118 (2014) 11752–11762.
[22] X. Cong, R.J. Kirkpatrick, ^{29}Si MAS NMR study of the structure of calcium silicate hydrate, Adv. Cem. Based Mater. 3 (1996) 144–156.
[23] T.F. Sevelsted, J. Skibsted, Carbonation of C–S–H and C–A–S–H samples studied by ^{13}C, ^{27}Al and ^{29}Si MAS NMR spectroscopy, Cem. Concr. Res. 71 (2015) 56–65.
[24] G.D. Miron, D.A. Kulik, Y. Yan, J. Tits, B. Lothenbach, Extensions of CASH+ thermodynamic solid solution model for the uptake of alkali metals and alkaline earth metals in C-S-H, Cem. Concr. Res. (2021). Submitted for publication.
[25] G.D. Miron, D.A. Kulik, E. Wieland, B. Lothenbach, Extensions of CASH+ thermodynamic solid solution model for Al(III) and Fe(III) uptake in C-S-H, Cem. Concr. Res. (2021). In preparation.
[26] G.D. Miron, D.A. Kulik, J. Tits, B. Lothenbach, Extensions of CASH+ thermodynamic solid solution model for uptake of cations of environmental concern in C-S-H (calcium silicate hydrate), Appl. Geochem. (2021). In preparation.
[27] B. Lothenbach, D.A. Kulik, T. Matschei, M. Balonis, L. Baquerizo, B.Z. Dilnesa, G. D. Miron, R. Myers, Cemdata18: a chemical thermodynamic database for hydrated

Portland cements and alkali-activated materials, Cem. Concr. Res. 115 (2019) 472–506.
[28] T. Thoenen, W. Hummel, U. Berner, E. Curti, The PSI/Nagra Chemical Thermodynamic Database 12/07, PSI Bericht, Paul Scherrer Institut, Villigen PSI, 2014.
[29] G.D. Miron, D.A. Kulik, S.V. Dmytrieva, T. Wagner, GEMSFITS: code package for optimization of geochemical model parameters and inverse modeling, Appl. Geochem. 55 (2015) 28–45.
[30] G.D. Miron, D.A. Kulik, T. Thoenen, Generating isocoulombic reactions as a tool for systematic evaluation of temperature trends of thermodynamic properties: application to aquocomplexes of lanthanides and actinides, Geochim. Cosmochim. Acta 286 (2020) 119–142.
[31] L. Glasser, H.D.B. Jenkins, Predictive thermodynamics for ionic solids and liquids, Phys. Chem. Chem. Phys. 18 (2016) 21226–21240.
[32] A.C.A. Muller, K. Scrivener, A.M. Gajewicz, P.J. McDonald, Densification of C−S−H measured by ^{1}H NMR relaxometry, J. Phys. Chem. C 117 (2013) 403–412.
[33] A.M. Gajewicz-Jaromin, P.J. McDonald, A.C.A. Muller, K.L. Scrivener, Influence of curing temperature on cement paste microstructure measured by 1H NMR relaxometry, Cem. Concr. Res. 122 (2019) 147–156.
[34] F. Avet, E. Boehm-Courjault, K.L. Scrivener, Investigation of C-A-S-H composition, morphology and density in limestone calcined clay cement (LC^3), Cem. Concr. Res. 115 (2019) 70–79.
[35] A.J. Allen, J.J. Thomas, H.M. Jennings, Composition and density of nanoscale calcium–silicate–hydrate in cement, Nat. Mater. 6 (2007) 311–316.
[36] J.J. Thomas, A.J. Allen, H.M. Jennings, Density and water content of nanoscale solid C–S–H formed in alkali-activated slag (AAS) paste and implications for chemical shrinkage, Cem. Concr. Res. 42 (2012) 377–383.
[37] J.J. Thomas, H.M. Jennings, A.J. Allen, Relationships between composition and density of tobermorite, jennite, and nanoscale CaO-SiO_2-H_2O, J. Phys. Chem. C 114 (2010) 7594–7601.
[38] I.G. Richardson, Model structures for C-(A)-S-H(I), Acta Crystallogr. B70 (2014) 903–923.
[39] J.E. Hurst, K. Harrison, Estimation of liquid and solid heat capacities using a modified Kopp's rule, Chem. Eng. Commun. 112 (1992) 21–30.
[40] J.A. Chermak, J.D. Rimstidt, Estimating the thermodynamic properties (ΔG^o_f and ΔH^o_f) of silicate minerals at 298 K from the sum of polyhedral contributions, Am. Mineral. 74 (1989) 1023–1031.
[41] T.J.B. Holland, Dependence of entropy on volume for silicate and oxide minerals: a review and a predictive model, Am. Mineral. 74 (1989) 5–13.
[42] S. Rudtsch, Uncertainty of heat capacity measurements with differential scanning calorimeters, Thermochim. Acta 382 (2002) 17–25.
[43] D.D. Wagman, W.H. Evans, V.L. Parker, R.H. Schumm, I. Halow, S.M. Bailey, K. L. Churney, R.L. Nuttall, The NBS tables of chemical thermodynamic properties: selected values for inorganic and C_1 and C_2 organic substances in SI units, J. Phys. Chem. Ref. Data 11 (1982) 336.
[44] J.G. Price, Ideal site mixing in solid solutions, with an application to two-feldspar geothermometry, Am. Mineral. 70 (1985) 696–701.
[45] B.J. Wood, J. Nicholls, The thermodynamic properties of reciprocal solid solutions, Contrib. Mineral. Petrol. 66 (1978) 389–400.
[46] B. Sundman, J. Ågren, A regular solution model for phases with several components and sublattices, suitable for computer applications, J. Phys. Chem. Solid 42 (1981) 297–301.
[47] M. Hillert, The compound energy formalism, J. Alloys Compd. 320 (2001) 161–176.
[48] D.A. Kulik, T. Wagner, S.V. Dmytrieva, G. Kosakowski, F.F. Hingerl, K. V. Chudnenko, U. Berner, GEM-Selektor geochemical modeling package: revised algorithm and GEMS3K numerical kernel for coupled simulation codes, Comput. Geosci. 17 (2013) 1–24.
[49] T. Wagner, D.A. Kulik, F.F. Hingerl, S.V. Dmytrieva, GEM-Selektor geochemical modeling package: TSolMod library and data interface for multicomponent phase models, Can. Mineral. 50 (2012) 1173–1195.
[50] H.C. Helgeson, D.H. Kirkham, G.C. Flowers, Theoretical prediction of the thermodynamic behavior of aqueous electrolytes at high pressures and temperatures: IV. Calculation of activity coefficients, osmotic coefficients, and apparent molal and standard and relative partial molal properties to 600 °C and 5 kb, Am. J. Sci. 281 (1981) 1249–1516.
[51] R.G. Berman, Mixing properties of Ca-Mg-Fe-Mn garnets, Am. Mineral. 75 (1990) 328–344.
[52] J.J. Chen, J.J. Thomas, H.F.W. Taylor, H.M. Jennings, Solubility and structure of calcium silicate hydrate, Cem. Concr. Res. 34 (2004) 1499–1519.
[53] E. L'Hopital, B. Lothenbach, G. Le Saout, D. Kulik, K. Scrivener, Incorporation of aluminium in calcium-silicate-hydrates, Cem. Concr. Res. 75 (2015) 91–103.
[54] E. L'Hopital, B. Lothenbach, K. Scrivener, D.A. Kulik, Alkali uptake in calcium alumina silicate hydrate (C-A-S-H), Cem. Concr. Res. 85 (2016) 122–136.
[55] J. Haas, A. Nonat, From C–S–H to C–A–S–H: experimental study and thermodynamic modelling, Cem. Concr. Res. 68 (2015) 124–138.
[56] S.W.W. Swanton, T.G.G. Heath, A. Clacher, Leaching behaviour of low Ca:Si ratio CaO–SiO_2–H_2O systems, Cem. Concr. Res. 88 (2016) 82–95.
[57] C. Roosz, P. Vieillard, P. Blanc, S. Gaboreau, H. Gailhanou, D. Braithwaite, V. Montouillout, R. Denoyel, P. Henocq, B. Made, Thermodynamic properties of C-S-H, C-A-S-H and M-S-H phases: results from direct measurements and predictive modelling, Appl. Geochem. 92 (2018) 140–156.
[58] G. Plusquellec, Analyse in situ de suspensions de silicate de calcium hydraté: application aux interactions ioniques à la surface des particules, Universite de Bourgogne, Dijon, France, 2014.
[59] P. Henocq, Modélisation des interactions ioniques à la surface des Silicates de Calcium Hydratés, Universite Laval, Quebec City, Canada, 2005.
[60] C.S. Walker, D. Savage, M. Tyrer, K.V. Ragnarsdottir, Non-ideal solid solution aqueous solution modeling of synthetic calcium silicate hydrate, Cem. Concr. Res. 37 (2007) 502–511.
[61] L. Nicoleau, E. Schreiner, Determination of Ca^{2+} complexation constants by monomeric silicate species at 25 °C with a Ca^{2+} ion selective electrode, Cem. Concr. Res. 98 (2017) 36–43.
[62] E. Bonaccorsi, S. Merlino, A.R. Kampf, The crystal structure of tobermorite 14 A (plombierite), a C-S-H phase, J. Am. Ceram. Soc. 88 (2005) 505–512.
[63] S. Merlino, E. Bonaccorsi, T. Armbruster, The real structure of tobermorite 11 Å: normal and anomalous forms, OD character and polytypic modifications, Eur. J. Mineral. 13 (2001) 577–590.
[64] E. Courault, Simulation experimentale des C-S-H dans les betons modernes: etude de la composition et des proprietes a l'equilibre dans des milieux complexes, PhD thesis, Universite de Bourgogne, France Universite de Bourgogne, Dijon, France, 2000.
[65] M. Atkins, F.P. Glasser, L.P. Moroni, J.J. Jack, Thermodynamic modelling of blended cements at elevated temperature (50–90 °C), in: Department of the Environment (UK), HMIP, 1994, p. 193.
[66] F.P. Glasser, M. Tyrer, K. Quillin, D. Ross, J. Pedersen, K. Goldthorpe, et al., The Chemistry of Blended Cement and Backfills Intended for Use in Radioactive Waste Disposal, Environment Agency, Bristol, UK, 1999, p. 333.
[67] R.J. Myers, E. L'Hôpital, J.L. Provis, B. Lothenbach, Effect of temperature and aluminium on calcium (alumino) silicate hydrate chemistry under equilibrium conditions, Cem. Concr. Res. 68 (2015) 83–93.
[68] T.J.B. Holland, R. Powell, An internally consistent thermodynamic data set for phases of petrological interest, J. Metamorphic Petrology 16 (1998) 309–343.
[69] Z. Xie, J. Walther, Wollastonite + quartz solubility in supercritical NaCl aqueous aolutions, Am. J. Sci. 293 (1993) 235–255.
[70] S.A. Stronach, F.P. Glasser, Modelling the impact of abundant geochemical components on phase stability and solubility of the CaO—SiO_2—H_2O system at 25°C: Na^+, K^+, SO_4^{2-}, Cl^- and CO_3^2, Adv. Cem. Res. 9 (1997) 167–181.
[71] L. De Windt, F. Marsal, E. Tinseau, D. Pellegrini, Reactive transport modeling of geochemical interactions at a concrete/argillite interface, Tournemire site (France), in: Physics and Chemistry of the Earth, Parts A/B/C, 2008, pp. S295–S305.
[72] P. Blanc, X. Bourbon, A. Lassin, E.C. Gaucher, Chemical model for cement-based materials: temperature dependence of thermodynamic functions for nanocrystalline and crystalline C–S–H phases, Cem. Concr. Res. 40 (2010) 851–866.
[73] M. Kersten, Aqueous solubility diagrams for cementitious waste stabilization systems. 1. The C-S-H solid-solution system, Environ. Sci. Technol. 30 (1996) 2286–2293.
[74] V.A. Sinitsyn, D.A. Kulik, M.S. Khororivsky, I.K. Karpov, Prediction of solid-aqueous equilibria in cementitious systems using Gibbs energy minimization: I. Multiphase aqueous ideal solution models, Mater. Res. Soc. Symp. Proc. 506 (1998) 953–960.
[75] B. Lothenbach, F. Winnefeld, Thermodynamic modelling of the hydration of Portland cement, Cem. Concr. Res. 36 (2006) 209–226.
[76] D.A. Kulik, M. Kersten, Aqueous solubility diagrams for cementitious waste stabilization systems. 4. A carbonation model for Zn-doped calcium silicate hydrate by Gibbs energy minimization, Environ. Sci. Technol. 36 (2002) 2926–2931.
[77] X. Gaona, D.A. Kulik, N. Macè, E. Wieland, Aqueous-solid solution thermodynamic model of U(VI) uptake in C-S-H phases, Appl. Geochem. 27 (2012) 81–95.
[78] A. Nonat, The structure and stoichiometry of C-S-H, Cem. Concr. Res. 34 (2004) 1521–1528.
[79] C. Labbez, A. Nonat, I. Pochard, B. Jönsson, Experimental and theoretical evidence of overcharging of calcium silicate hydrate, J. Colloid Interface Sci. 309 (2007) 303–307.
[80] J.E. Rossen, B. Lothenbach, K. Scrivener, Composition of C–S–H in pastes with increasing levels of silica fume addition, Cem. Concr. Res. 75 (2015) 14–22.
[81] E. Tajuelo Rodriguez, I.G. Richardson, L. Black, E. Boehm-Courjault, A. Nonat, J. Skibsted, Composition, silicate anion structure and morphology of calcium silicate hydrates (C-SH) synthesised by silica-lime reaction and by controlled hydration of tricalcium silicate (C3S), Adv. Appl. Ceram. 114 (2015) 362–371.
[82] C. Tournassat, A. Neaman, F. Villieras, D. Bosbach, L. Charlet, Nanomorphology of montmorillonite particles: estimation of the clay edge sorption site density by low-pressure gas adsorption and AFM observations, Am. Mineral. 88 (2003) 1989–1995.
[83] P.H. Santschi, P.W. Schindler, Complex formation in the ternary systems Ca^{II}–H_4SiO_4–H_2O and Mg^{II}–H_4SiO_4–H_2O, J. Chem. Soc. Dalton Trans. 2 (1974) 181–184.
[84] D. Kulik, Minimising uncertainty induced by temperature extrapolations of thermodynamic data: A pragmatic view on the integration of thermodynamic databases into geochemical computer codes, in: The Use of Thermodynamic Databases in Performance Assessment, 2002, pp. 125–137.

Glossary

Symbol: Meaning
BT: Bridging tetrahedral site (sublattice) in C-S-H structure
BTI: Combined BT and IC sites used in CSHQ and CSH3T models [4]
C/S: Ca/Si mole ratio in the system, in bulk cement or in C-S-H
$[Ca]_{aq}$: Total dissolved aqueous concentration of Ca (molal or molar)

DSP: Discrete Solid Phase (solid solution model) approximation
DU: Dimeric (calcium) unit in C-S-H structure
GEM: Gibbs energy minimization [method, software]
H/S: H_2O/Si mole ratio in C-S-H solid
IC: Interlayer Cationic site (sublattice) in C-S-H structure
IW: Interlayer Water site (sublattice) in C-S-H structure
MC: Monte Carlo [sampling or calculations]
MCL: Mean (silicate) chain length [in defect-tobermorite structure]
[Si]$_{aq}$: Total dissolved aqueous concentration of Si (molal or molar)
sublattice: Set of all structural sites of the same type in the (crystal) structure
TDB[Chemical]: thermodynamic database
VBT: Volume-based thermodynamics [predictions]
G°_{298}: Standard molar Gibbs energy (of formation) at 25 °C (298.15 K; other standard thermodynamic properties are given in a similar notation, e.g. the standard enthalpy H°_{298})
δG°_{298}: 95% (two-sigma) confidence interval of G°_{298} value
G^*_{298}: Initially estimated/predicted G°_{298} value [of a CASH+ endmember]
logK°_{298}: Equilibrium constant of reaction at 25 °C (298.15 K), 1 bar
$^{BT}W_{CS}$: Berman symmetric interaction parameter for C and S in BT sites
$^{IC}W_{Cv}$: Berman symmetric interaction parameter for C and v in IC sites